Collagen 17A1 in the urothelium regulates epithelial cell integrity and local immunological responses in obstructive uropathy

Takashi Namba[1], Osamu Ichii[1,2]*, Ken Natsuga[3], Teppei Nakamura[4], Yuki Otani[1], and Yasuhiro Kon[1]

[1]Laboratory of Anatomy, Department of Basic Veterinary Sciences, Faculty of Veterinary Medicine, Hokkaido University, Sapporo, Hokkaido, Japan 060-0818

[2]Laboratory of Agrobiomedical Science, Faculty of Agriculture, Hokkaido University, Sapporo, Hokkaido, Japan 060-8589

[3]Department of Dermatology, Faculty of Medicine and Graduate School of Medicine, Hokkaido University, Sapporo, Hokkaido, Japan 060-8638,

[4]Laboratory of Laboratory Animal Science and Medicine, Department of Applied Veterinary Sciences, Faculty of Veterinary Medicine, Hokkaido University, Sapporo, Hokkaido, Japan 060-0818

*Corresponding author: Osamu Ichii, D.V.M., Ph.D.

Laboratory of Anatomy, Department of Basic Veterinary Sciences, Faculty of Veterinary Medicine, Hokkaido University, Kita 18-Nishi 9, Kita-ku, Sapporo, Hokkaido, 060-0818, Japan

Tel & Fax: +81-11-706-5188, Email: ichi-o@vetmed.hokudai.ac.jp

RUNNING TITLE:

Collagen 17A1 sets urothelial integrity

ABBREVIATIONS:

Actb, beta-actin; α-SMA, alpha smooth muscle actin; BrdU, bromodeoxyuridine; BSA, bovine serum albumin; COL17A1, collagen 17A1; CK14, cytokeratin-14; d, day; FGFR2, fibroblast growth factor receptor 2; GO, gene ontology; IF, immunofluorescence; IHC, immunohistochemistry; Itgam, integrin alpha M; KO, knock out; OCLN, occludin; PBS, phosphate-buffered saline; PDGFRα, platelet-derived growth factor receptor alpha; qPCR, quantitative polymerase chain reaction; RP, renal pelvis; SE, standard error; Sham, sham-operation; TEM, transmission electron microscopy; TJP, tight junction protein; Upk2, uroplakin 2; UTALS, urinary tract-associated lymphoid structure; UUO, unilateral ureteral obstruction; WT, wild-type; ZO-1, zonula occludens-1.

FUNDING

This work was supported in part by the Japan Society for the Promotion of Science (grant numbers: JP20J22559, JP19K22352, and JP21H04751).

CONFLICT OF INTEREST STATEMENT

The authors have no competing interests to declare.

ABSTRACT

Collagen 17A1 (COL17A1), an epidermal hemidesmosome component, is ectopically induced in the urothelium of mouse and human renal pelvis (RP) in parallel with urinary-tract-associated lymphoid structure development. Here, we found that COL17A1 was induced in obstructive-uropathy-prone ureter of humans and cats. To ascertain its function, murine urinary organs with unilateral ureteral obstruction (UUO) were analyzed during one week after surgery. One day after UUO, COL17A1 expression increased in urothelial cells of RP and ureter, and was positively correlated with renal tubulointerstitial lesions. A portion of RP where the smooth muscle layer from the ureter was interrupted was sensitive to urothelium deciduation and COL17A1 induction, showing urine leaked from the RP lumen into the parenchyma. After urine stimulation, cultured immune cells expressed *Cxcl2*, also upregulated in $CD11b^+$ cells following COL17A1 stimulation. One day after UUO, $CXCL2^+$ $CD11b^+$ cells infiltrated the urothelium-disrupted area; however, these numbers were significantly lower in *Col17a1*-deficient mice. $COL17A1^+$ urothelial cells partially co-expressed CK14, a progenitor cell marker for urothelium, while *Col17a1*-deficient mice had lower numbers of $CK14^+$ cells. Gene Ontology analysis revealed that expression of epithelial- and immune-associated genes was up- and down-regulated, respectively, in the ureter of *Col17a1*-deficient mice four days after UUO. Thus, COL17A1 maintains urothelium integrity by regulating urothelial cell adhesion, proliferation and differentiation, and activates local immune responses during obstructive uropathy in mammals.

Keywords: collagen 17A1, urothelium, ureter, renal pelvis, urine, inflammation, obstructive uropathy

INTRODUCTION

The collagen family including 28 members is divided into fibrillar and non-fibrillar types; the former forms the fibril networks of the extracellular matrix, while the latter forms trans- and basement membranes and connects to the surface of collagen fibrils[1]. Collagen 17A1 (COL17A1, also known as BP180), belonging to the non-fibrillar collagen type, is a transmembrane structural component of hemidesmosomes, is constitutively expressed in keratinocytes, and attaches the epidermis to the basement membrane[2]. The gene has been identified as a causal gene for junctional epidermolysis bullosa[2]. Pathologically, COL17A1 can be an autoantigen for bullous pemphigoid, and is overexpressed in epidermal basal cells during wound healing in the context of cell migration and proliferation[3–5]. In the urothelium, COL17A1 has been detected in the urinary bladder of cows and rats; however, its function in urothelium has not been well investigated[6].

Recently, we revealed that COL17A1 is ectopically induced in renal pelvis (RP) urothelium overlaying urinary tract-associated lymphoid structures (UTALSs) in mice and humans with chronic nephritis[7]. UTALSs, tertially lymphoid structures developing under the urothelium, are induced and stimulated by the production of cytokines and chemokines in immune and stromal cells of RP, as well as by urine leakage from RP lumen to parenchyma. Moreover, UTALS development is affected by aging and systemic immune conditions and is positively correlated with the progression of renal lesions. Our previous results indicated that COL17A1 in RP is induced via the FOS/JUN pathway and plays a role in

76 UTALS development by stimulating the production of IL-6, IL-22, and CXCL9 from UTALS-forming
77 cells[7].

78 We also reported urine-urothelial barrier disruption in RP of mice and humans with chronic nephritis,
79 along with urine leakage from the RP lumen into parenchyma in our murine model[7]. Urothelium injuries
80 are observed owing to urinary stasis in several diseases, including obstructive nephropathy[8]. Mammalian
81 urinary tracts can be obstructed by anatomical defects, urolithiasis, bacterial infections, and cystitis, as
82 well as neoplasia. Disorders of upper urinary tract elements including RP and ureter can lead to various
83 degrees of hydronephrosis[9]. The prevalence of urolithiasis in humans is increasing globally with a range
84 from 1–13% depending on obstructive position[10]. In neonates and infants, the ureteropelvic junction can
85 be a major site of obstruction in the urinary tract due to a characteristic anatomical abnormality reported
86 for 1 in 1,500 live births[11]. A few studies have shown that injured urothelium is characterized by cell
87 proliferation, flattened cell shape, and disrupted tight junctions[12,13]. However, no prior report has clearly
88 outlined the characteristics of urine-urothelial barrier disruption, subsequent pathological events, or
89 crucial molecules in urinary tract obstruction-related diseases, placing a special focus on the role of urine.

90 Here, we aimed to clarify the relationship between urine leakage induced by urine-urothelial barrier
91 disruption and local immune responses and assess the role of COL17A1 by analyzing RP and ureter in
92 unilateral ureteral obstruction (UUO)-injured mice. Importantly, COL17A1 ectopic expression is also

present in obstructed ureters in both human and feline cases, indicating its usefulness as a novel indicator for urine-urothelial barrier disruption.

MATERIALS AND METHODS

Human sample analysis

Ten percent neutral buffered formalin-fixed and paraffin-embedded normal and diseased ureter (female Caucasian, 58- and 60-year-old, respectively) were obtained from KAC (Kyoto, Japan). Sections were used for Masson's trichrome staining and immunohistochemistry (IHC) targeting COL17A1 and CD11b.

Cat sample analysis

Normal ureters were obtained from healthy cats euthanized in other experiments. Diseased ureters, surgically resected from the obstructed lesion to the ureter-urinary bladder junction were collected from cats manifesting obstructive urolithiasis at the Matsubara Animal Hospital (Osaka, Japan). All ureters were fixed using 10% neutral buffered formalin (n = 5 in each group). For *in situ* hybridization, paraffin sections (5-μm thick) were assessed using an RNAscope 2.5 HD Reagent Kit-BROWN (Advanced Cell Diagnostics, Inc., Hayward, CA, USA) with custom-ordered probe-Fc-*COL17A1*, positive control probe-Fc-*PPIB*, and negative control probe-*DapB*. The images of positive and negative controls are shown in Supplementary Fig. S1.

Mouse sample preparation

Two-month-old C57BL/6N and six-month-old MRL/MpJ mice were purchased from Japan SLC

(Hamamatsu, Japan), and three-month-old *Col17a1*-deficient (knock out; KO) mice (C57BL/6N background) were maintained in our faculty under specific pathogen-free conditions. The *Col17a1*-KO mice used in this study have been previously described[14–17]. Briefly, replaced regions of exon 2 in the gene result in missing downstream exon sequences and in a homozygous deletion. The mice show blisters and erosions induced by trauma, blister healing delay, absence of hair follicles, and high mortality rates (80.1% within 8 weeks after birth). For C57BL/6N, the UUO group was assessed for 1, 4, 7, or 28 days (d) after UUO induction, and an equivalent sham-operation (Sham) group was prepared (n = 4 or 5). UUO at 1 d was performed in *Col17a1*-KO (n = 4 or 5). Briefly, the right ureter was ligated at the part caudal to the caudal end of the kidney, and the hilum of the kidney and the ureter region cranial to the ligated site were evaluated for the histopathology of RP and ureter, respectively. Bromodeoxyuridine (BrdU, 0.1 mg/g), a proliferation marker, was administered to C57BL/6N with UUO and Sham two hours before sample collection. Under deep anesthesia using a mixture of medetomidine (0.3 mg/kg), midazolam (4 mg/kg), and butorphanol (5 mg/kg), mice were euthanized by cervical dislocation.

Histopathology

Kidneys and ureters were collected and fixed using 4% paraformaldehyde. Histological paraffin sections (2-μm thick) were stained using Masson's trichrome and periodic acid Schiff and hematoxylin staining (PAS-H). Either IHC or immunofluorescence (IF) was performed as previously described[18]. Information

132 regarding immunostaining is given in Table 1. Stained sections were examined using a BZ-X710
133 microscope (Keyence, Osaka, Japan) and converted to virtual slides using NanoZoomer 2.0-RS
134 (Hamamatsu Photonics, Shizuoka, Japan).

135 The luminal area of the ureter was measured, and the average was calculated in five sections from
136 each mouse using NDP.View2.

137 For the IHC sections, the relative COL17A1^{+} area in the examined area of urothelium was measured
138 using a BZ-X Analyzer (Keyence). This measurement was performed in three regions; thick and thin RP,
139 defined by the presence or absence of smooth muscle layers, and ureter. The ureter luminal area was also
140 measured. Consecutive lengths of COL17A1^{+} cells were measured from the junction between thin and
141 thick RP to each portion. To evaluate RP histology in *Col17a1*-KO, the numbers of urothelial cells,
142 cytokeratin-14 (CK14)$^{+}$ urothelial cells, and CD11b^{+} cells under the urothelium were counted in the
143 urothelial region frequently expressing COL17A1 (400 μm length from the RP junction to the thick
144 portion). For quantification of cell infiltration into tubulointerstitium, the numbers of CD11b^{+} cells were
145 counted in 20 tubulointerstitial areas at 400× magnification using NDP.view2, and averages per area were
146 calculated[19]. To evaluate IL-36α, which was expressed in injured distal tubules, the numbers of IL-36α^{+}
147 tubules in the cortex area were counted in three sections from each individual, and then the averages were
148 divided by the area examined[18,20].
149

Transmission electron microscopy (TEM)

Small pieces of kidney tissues including RP taken 1 d after UUO were pre-fixed using 4% paraformaldehyde/0.1 M cacodylate buffer containing 2.5% glutaraldehyde for 2 h at room temperature. The specimens were processed using the osmium-thiocarbohydrazide-osmium method. First, samples were washed five times using 0.1 M cacodylate buffer and block-stained using 1.5% potassium ferrocyanide/2% OsO_4/0.1 M cacodylate buffer for 1 h at 4 °C. After washing four times in distilled water, specimens were block-stained using 1% thiocarbohydrazide solution for 20 min at room temperature and washed again. They were then post-fixed using 2% OsO_4 for 30 min at room temperature, washed again, and stained using 1% uranyl acetate overnight at 4 °C. After washing four times in distilled water, specimens were block-stained using 0.4% L-aspartic acid/0.66% lead nitrate solution for 30 min at 60 °C followed by four washes with distilled water. Next, specimens were dehydrated using a series of ethanol concentrations (30-95%) for 10 min each at 4 °C. After being dehydrated three times in 100% ethanol at 4 °C, specimens were soaked in a 1:1 (v/v) mixture of 100% ethanol and QY-1 for 10 min at room temperature, and subsequently twice in QY1 for 30 min at room temperature. Next, specimens were soaked in a 1:1 (v/v) volume mixture of QY-1 and Epon 812 (#R1078; TAAB, Berkshire, England) for 1 h at room temperature followed by Epon 812 overnight at room temperature. After exchanging the resin and holding the specimens at room temperature for 1 h, specimens were embedded and polymerized in fresh Epon 812 for 48 h at 60 °C. Ultrathin sections (60 nm) were imaged using a JEOL TEM

(JEM-1400plus; JEOL, Tokyo, Japan).

Urothelium integrity analysis

We used our previous method with modifications[7]. Firstly, UUO was generated using a vascular clip (KN-353-AS-1-40 g; Natsume Seisakusho, Tokyo, Japan) that was released after 1 d. Evans blue (5 mg/mL; #E2129; Merck, Kenilworth, NJ, USA) was mixed with bovine serum albumin (BSA; 40 mg/mL), incubated for 30 min, and filtered using a 0.22 μm syringe filter to produce Evans blue-conjugated BSA solution. The urethra of mice was ligated under combined anesthesia (0.3 mg/kg medetomidine, 4.0 mg/kg midazolam, and 5.0 mg/kg butorphanol), and a 21 G butterfly needle was inserted from the apex of the urinary bladder and fixed via ligation. After clamping one ureter using vascular clips, 50 μL of Evans blue-conjugated BSA was injected into the urinary bladder through the inserted needle. Evans blue-conjugated BSA injection into RP was confirmed via a color change in the other ureter. After 5 min of contact time, kidneys were collected and embedded in optimal cutting temperature compound (#4583; Sakura Finetek Japan, Tokyo, Japan) using liquid nitrogen. Frozen sections (4 μm-thick) were prepared and air-dried. Finally, Evans blue-conjugated BSA fluorescence was observed using a BZ-X710 microscope and the Cy5 filter (Keyence).

Cell culture

Mimic lymphoid structures were prepared as previously described[7]. The spleen of a 6-month-old male MRL/MpJ mouse was collected and minced in a culture dish. Next, 10 mL of 1× phosphate-buffered saline (PBS; #164-25511; FUJIFILM Wako, Osaka, Japan) was added, after which the sample was filtered using 100 μm cell strainers (#352360; Corning Inc., Corning, NY, USA) and centrifuged at 210 g for 5 min. After aspiration of supernatant, cells were resuspended, incubated with 10 mL 0.017 M Tris buffer containing 0.75% ammonium chloride (pH 7.65) for 5 min, and washed with 10 mL PBS. This solution was filtered using 40 μm cell strainers (#352340; Corning Inc.) and centrifuged at 1 000 rpm for 5 min. After washing twice with PBS, the collected cells were resuspended in RPMI-1640 with L-glutamine (#189-02025; FUJIFILM Wako) without antibiotics and harvested in 24-well culture plates (#92424; Techno Plastic Products, Trasadingen, Switzerland).

Cells were defined as mimic lymphoid structures containing immune and stromal cells. Some spleen cells were collected similarly without ammonium chloride treatment, and T, B, and $CD11b^+$ cells were separately isolated using magnetic-activated cell sorting commercial kits (EasySep, #ST-19851RF, #ST-19854RF, #ST-18970RF; VERITAS, Santa Clara, CA, USA). The mimic lymphoid structures or separated cells were stimulated using recombinant human COL17A1 (0.4 μg/mL, rhCOL17A1; #MBS1265558; MyBioSource, San Diego, CA, USA) or BSA (0.4 μg/mL, #013-27054; FUJIFILM Wako). Endotoxin levels in rhCOL17A1 were <1.0 endotoxin unit per 1.0 μg protein as determined using a limulus amebocyte lysate test (MyBioSource). Urine was collected from six male MRL/MpJ mice at 6

months of age via compressive urination, after which samples from each strain were pooled and centrifuged at 1 500 rpm for 5 min. The urine supernatant was filtered using a 0.22 μm syringe filter (#SLPES2522S; Hawach Scientific, Shaanxi, China), diluted 1:4 with PBS, and used for mimic lymphoid structure stimulation. Mimic lymphoid structure or isolated cell experiments were performed using 2.5×10^7 cells/mL and 500 μL medium/well or 1.25×10^6 cells/mL and 500 μL medium/well, respectively, and samples were stimulated with urine, rhCOL17A1, BSA, or PBS, and then collected for RNA analysis.

Microarray

Total RNA was purified from mouse cultured cells and tissues stored in RNA later using the RNeasy Mini Kit (Qiagen, Hilden, Germany). For mimic lymphoid structures, RNA from PBS- or MRL/MpJ urine-treated groups (n = 5) was pooled into a single sample for each group to evaluate chemokine expression in mimic lymphoid structures. The RNA of ureters was prepared from *Col17a1*-KO or WT mice 4 d after UUO (n = 3) to comprehensively analyze altered gene expression in the ureter. RNA integrity was validated using an Agilent 2100 Bioanalyzer II (Agilent Technologies, Santa Clara, CA, USA). Complementary DNA was synthesized using a Low Input Quick Amp Labeling Kit (Agilent Technologies), and gene expression was analyzed using an Agilent Technologies Microarray Scanner and SurePrint G3 Mouse 8x60K ver.2.0 (Agilent Technologies). Raw data was normalized using 75Percentile Shift (GeneSpring; Agilent Technologies). Gene Ontology Resource (https://geneontology.org/;

2023-10-15) was used for Gene Ontology (GO) analysis of the ureter. The data were deposited in the NCBI Gene Expression Omnibus (https://www.ncbi.nlm.nih.gov/geo/; GEO Series accession numbers GSE207999 and GSE222953).

Quantitative polymerase chain reaction (qPCR)

Kidney and ureter 1 d after UUO and non-injured collateral samples were preserved using an RNAlater solution (#R0901; Merck KgaA, Darmstadt, Germany). RPs were manually isolated from kidneys through microdissection under a stereo microscope as reported previously[7]. Total RNA from these specimens and mimic lymphoid structures was purified using TRIzol reagent (#15596018; Thermo Fisher Scientific) following the manufacturer's instructions. Purified total RNA was used as a template to synthesize cDNA using the ReverTra Ace qPCR RT Master Mix with gDNA Remover (#FSQ-301; Toyobo, Osaka, Japan). qPCR analysis was performed on cDNA (20 ng/μL) using the THUNDERBIRD SYBR qPCR Mix (#QPS-101; Toyobo), gene-specific primers (Table 2), and a real-time thermal cycler (CFX Connect; BIO-RAD, Santa Rosa, CA, USA). qPCR cycling conditions were 95 °C for 1 min, 95 °C for 15 s, and 60 °C for 45 s (40 cycles). Data were normalized based on values for beta-actin (*Actb*).

Statistical analysis

The results are expressed as mean ± standard error (SE) and statistically analyzed in a non-parametric

manner. Differences between the two groups were analyzed using the Mann–Whitney *U*-test. Differences among three or more groups were analyzed using the Kruskal–Wallis test followed by Scheffé's method. Correlation between the two parameters was analyzed using Spearman's correlation test. $P < 0.05$ was considered statistically significant.

Ethics statement

The study of human samples was approved by the Ethics Committee of the Faculty of Veterinary Medicine and International Institute for Zoonosis Control, Hokkaido University (approval no. 29-5). Collection of samples from human subjects was performed in accordance with the Declaration of Helsinki and the Declaration of Istanbul. All animal experimentation was approved by the Institutional Animal Care and Use Committee of the Faculty of Veterinary Medicine, Hokkaido University (approved by the Association for Assessment and Accreditation of Laboratory Animal Care International, approval no. 21-0008 for mice, 14-0054, 20-0081 for cats).

RESULTS

COL17A1 expression in the ureter of humans and cats with urolithiasis

Our previous study demonstrated that COL17A1 was expressed in human RP urothelium with infectious pyelonephritis and non-infectious chronic nephritis[7]. Here, we examined COL17A1 expression in the human ureter with urolithiasis. Cats, which also show a high susceptibility to urinary tract obstruction (incidence 7–8%), were also analyzed[21,22]. Compared with healthy ureters, diseased (urolithiasis) ureters of both humans and cats presented a dilated lumen, abundant collagen fibers, and immune cell infiltration in the lamina propria and submucosa. Cell aggregation was observed in the human ureter (Fig. 1A). In a human ureter showing normal histology, COL17A1 was detected at low levels in the basal portion of the urothelium, whereas in a diseased ureter with urolithiasis, $COL17A1^+$ reactions were more prevalent and immune cell aggregation was observed (Fig. 1B). In both healthy and diseased ureter of cats, $COL17A1^+$ reactions were observed in the basal portion of the urothelium and were highly abundant in each cell in diseased ureter (Fig. 1C), indicating that COL17A1 expression dynamics are common between different species.

COL17A1 ectopic expression in ureter urothelium of UUO mice

COL17A1 expression was also examined in the ureter of UUO-injured C57BL/6N mice, in which hydroureteronephrosis with ureter luminal expansion, smooth muscle layer degradation, and an increase

273 in collagen fibers was marked from 4 d onwards (Supplementary Fig. S2). Although COL17A1 localized
274 in the basal portion of UUO-injured ureter urothelium from 1 d (but not in Sham), COL17A1$^+$ urothelium
275 and histological scores from IHC increased significantly from 4 d onwards (Fig. 2A and B). Further, the
276 luminal size of the ureter as well as renal histopathological scores, including for CD11b$^+$ myeloid cells in
277 tubulointerstitium and IL-36α$^+$ injured distal tubules, increased significantly in a time-dependent manner
278 following UUO induction (Supplementary Fig. S3), and was positively correlated with urothelium
279 COL17A1$^+$ scores (Fig. 2C).

280 The integrity of the urine-urothelial barrier was evaluated in the ureter after UUO. Histologically,
281 urothelial cell deciduation in the ureter was apparent from 4 d onwards, in parallel with COL17A1
282 overexpression (Fig. 2D). mRNA expression of epithelium-associated genes, uroplakin 2 (*Upk2*) and tight
283 junction protein 1 (*Tjp1*), but not occludin (*Ocln*), was significantly lower in isolated ureter at 7 d after
284 UUO than in collateral control (Fig. 2E). TJP1 (also known as zonula occludens-1; ZO-1), which was
285 observed in the apical portion of Sham ureter, was partially absent in UUO urothelium. The OCLN$^+$
286 reaction was transiently increased in ureter urothelium 4 d after UUO, and both OCLN-faint and
287 -overexpressing cells were observed at 7 d (Fig. 2F). Moreover, COL17A1 was expressed at low levels in
288 BrdU-incorporating cells (Fig. 2G), indicating an association with urothelium reconstruction after UUO.
289

290 **Migration and activation of CD11b$^+$ cells stimulated by urine and COL17A1**

291 Urine can stimulate the production of cytokines and chemokines by fibroblasts and immune cells[7]. Based
292 on our histopathological results, we hypothesized that urine-urothelial barrier disruption and subsequent
293 urine leakage due to UUO led to an immune response in ureter parenchyma.

294 Table 3 summarizes microarray data analyzing the urine-stimulated mimic lymphoid structures and
295 focusing on chemokine genes. Expression of *Cxcl2*, *Cxcl11*, *Cxcl12*, *Cxcl10*, *Ccl6*, *Cxcl13*, *Ccl1*, and
296 *Ccl25* in mimic lymphoid structures stimulated by urine was twice that in PBS-stimulated structures.
297 qPCR analysis of ureter with UUO indicated that of the chemokine genes assessed *Cxcl2* expression is
298 significantly higher in UUO samples at 7 d than in collateral controls (Table 3, Fig. 3A).

299 In diseased RP, COL17A1 can also serve as an immune stimulator[7]. Separately isolated murine B, T,
300 and $CD11b^+$ cells were stimulated using rhCOL17A1, and *Cxcl2* expression was analyzed. Following
301 rhCOL17A1 stimulation, *Cxcl2* expression was significantly upregulated in T and $CD11b^+$ cells compared
302 to expression following BSA stimulation. $CD11b^+$ cells showed the highest values among the cell types
303 examined (Fig. 3B). Histologically, $CXCL2^+$ cells aggregated beneath disrupted $ZO\text{-}1^+$ epithelial cells,
304 and $COL17A1^+$ urothelium was also observed close to these areas (Fig. 3C). Importantly, $CXCL2^+$
305 reactions co-localized with $CD11b^+$ cells (Fig. 3C). Expression of inflammatory and fibrotic genes (*Il1b*,
306 *Il6*, and *Tgfb*) was significantly higher in ureter of 7 d UUO samples than in collateral controls (Fig. 3D).
307 Moreover, most $CD11b^+$ cells were $Gr\text{-}1^+$ neutrophils and $IBA1^+$ macrophages even though no bacterial
308 infection was observed in the area (Supplementary Fig. S4A and S4B). Additionally, $CD11b^+$ cells

infiltrated the lamina propria and submucosa in the diseased ureter of humans and cats with urolithiasis (Supplementary Fig. S4C). The findings indicate that urine and COL17A1 can stimulate CXCL2 expression in $CD11b^+$ cells infiltrating the UUO ureter.

COL17A1 overexpression in RP urothelium of mice from 1 d after UUO

To identify the site of initiation of COL17A1 expression in the upper urinary tract after UUO, we also examined RP. UUO-injured RP showed an increase in collagen fibers from 4 d (Supplementary Fig. S5A). Mouse thin and thick RP urothelium were separately analyzed[23]; the former has one or two urothelial layers, lacks a smooth muscle layer, and covers the inner stripe of the renal outer medulla, whereas the latter, covering the cortex and connecting to the ureter, has two or three urothelial layers with an α-smooth muscle actin $(\alpha\text{-SMA})^+$ smooth muscle layer (Fig. 4A). As expected, few $COL17A1^+$ urothelial cells were observed at the junction between the thin and thick RP urothelium on the outer stripe of the renal outer medulla in the Sham group (Supplementary Fig. S5B), indicating COL17A1 expression during normal urothelial turnover.

In contrast, COL17A1 was clearly present in the basal portion of RP urothelium from 1 d after UUO (Fig. 4B), and $COL17A1^+$ urothelial cell numbers increased in thin and thick RP from 4 d onwards (Fig. 4B and C). The UUO 1 d group also showed urothelial disruption with decreasing platelet-derived growth factor receptor alpha $(PDGFR\alpha)^+$ fibroblasts (Fig. 4C). In RP isolated at 1 d, *Col17a1* expression was

significantly higher than in the collateral control, indicating that *Col17a1* mRNA was induced earlier here than in ureter, as no significant *Col17a1* expression was observed in ureter at 1 d (Fig. 4D). At 1 d after UUO, the consecutive length of COL17A1^{+} urothelial cells from the RP junction to the thick portion was greater than in thin RP (Fig. 4E). Urothelial COL17A1^{+} scores were significantly higher in the thick RP at 1 d compared with in Sham and increased in a time-dependent manner following UUO induction in both thick and thin RP. Further, COL17A1^{+} scores in both RP urothelia at 7 d UUO were significantly higher than in Sham (Fig. 4F). Importantly, COL17A1 expression in RP urothelium, especially the thick portion, was positively correlated with renal histopathological scores (Fig. 4G).

Consistent with our previous findings that the FOS/JUN pathway induced COL17A1 expression in RP urothelium[7], both FOS and JUN localized in the urothelial cell nuclei at the beginning of the thick RP (Fig. 4H), indicating that this is a crucial site for the initiation of COL17A1 expression after obstructive uropathy.

At 28d UUO, RP urothelium continued to express COL17A1; however, levels were diminished in the ureter urothelium with the progression of fibrosis (Supplementary Fig. S5C).

Altered integrity of the urine-urothelial barrier in RP urothelium post UUO

Urine-urothelial barrier integrity was evaluated in RP at 1 d UUO, when deciduation of urothelial cells was present at the junction between thin and thick RP (Fig. 5A). Consistent with results for ureters at 7 d

UUO, mRNA levels of *Upk2* and *Tjp1* were significantly decreased in the UUO ureter at 1 d compared to collateral controls, whereas *Ocln* showed a decreasing tendency in the UUO RP ($P = 0.063$; Fig. 5B). For IF in Sham, ZO-1 localized at the apical portion of RP urothelium, whereas OCLN localized at the apical and basal portions (Fig. 5C). On day 1, ZO-1$^+$ reactions were partially faint and OCLN localized mainly at the basal portion. Furthermore, these reactions clarified the partial disruption of urothelium at the RP junction. Although OCLN$^+$ intensity partially increased at 4 d, both tight junction proteins decreased at 7 d (Fig. 5C).

We assessed COL17A1 co-localization with CK14 and CD44; the former is a marker for urothelial progenitor cells, while the latter is a receptor for hyaluronic acid, laminin, collagen or fibronectin and a marker for urothelial cell proliferation as well as immune cell activation[24–26]. In Sham RP, CK14$^+$ urothelial cells were found and partially co-expressed COL17A1, whereas RP urothelium at 1 d UUO showed an increase in COL17A1$^+$ CK14$^-$ CD44$^+$ urothelial cells as well as low number of COL17A1$^+$ CK14$^+$ CD44$^+$ cells. From 4 d onwards, COL17A1$^+$ CK14$^+$ CD44$^+$ and COL17A1$^-$ CK14$^-$CD44$^+$ urothelial cells were prominent (Fig. 5D).

In TEM observation of RP urothelium at 1 d, folded apical membrane, abundant lysosomes, and ectopic red blood cells beneath the basement membrane were noted, distinct from collateral controls (Fig. 5E). Characteristically, urothelial cells had increased intracellular spaces and their cell processes extended to the lamina propria to interact with cells in the smooth muscle layer. Further, one cell migrated from the

363 lamina propria to the partially effaced basement membrane (Fig. 5E).

364 To further investigate urine-urothelial barrier integrity, Evans blue-conjugated BSA from the urinary

365 bladder was administered to RP as previously described[7]. Although urothelium of the collateral kidney

366 retained Evans blue-conjugated BSA in the lumen of the RP, following UUO Evans blue-conjugated BSA

367 leaked into RP parenchyma after 1 d; thus, suggesting dysfunction of the urine-urothelial barrier (Fig.

368 5F).

369

370 **Aggregation of CXCL2$^+$ CD11b$^+$ cells induced in UUO-injured RP**

371 Similar to ureters, expression of *Cxcl2* was significantly higher in 1 d RP than in collateral controls (Fig.

372 6A). Histologically, CXCL2$^+$ cells aggregated beneath the RP urothelium-leakage area induced by UUO

373 (Fig. 6B). In RP 1 d after UUO, expression of integrin alpha M (*Itgam*, encoding CD11b) was

374 significantly higher compared to in collateral controls although *Cd3e* expression was lower (Fig. 6C).

375 Histologically, there were few B220$^+$ B cells and CD3$^+$ T cells beneath RP urothelium at all time points

376 (Supplementary Fig. S6). CD11b$^+$ cells were observed to migrate to the lamina propria in RP at 1 d,

377 especially near the beginning of the thick RP, with lower numbers at 4 d, while numbers of collagen fibers

378 increased (Fig. 6D, Supplementary Fig. S5A). Consistent with our ureter results, CXCL2$^+$ reactions were

379 co-localized with CD11b$^+$ cells beneath COL17A1$^+$ urothelium in 1 d UUO samples (Fig. 6E).

380 Furthermore, mRNA levels of *Il1b*, *Il6*, and *Tgfb* were significantly higher in RP of 1 d UUO samples

compared to in collateral controls (Fig. 6F).

Abnormal urothelium morphology and inhibition of immune cell infiltration in RP of *Col17a1*-KO mice post UUO

For further investigation into COL17A1 functions in UUO pathology, *Col17a1*-KO mice were used. The ureter of *Col17a1*-KO 4 d after UUO was examined using a microarray followed by GO analysis, due to ease of sample collection and given that this was a known time point of COL17A1 overexpression in the ureter. In *Col17a1*-KO, epithelium- and immune-related GO terms were detected in genes with up- and downregulated expression, respectively (Table 4, Supplementary Table S1). Genes with upregulated expression included urothelium-expressed genes, *Krt14* (encoding CK14) and *Upk1b* (Supplementary Fig. S7), indicating that COL17A1 dysfunction affected urothelial integrity and local immunity.

RP histopathology of *Col17a1*-KO 1 d was assessed as RP urothelium showed early induction of COL17A1 from 1 d UUO. At the RP junction, urothelial disruption and urothelial cell proliferation were observed; however, infiltrating cell numbers were lower in *Col17a1*-KO than in WT (Fig. 7A). In the RP histology of collateral kidney, superficial urothelial cells partially presented pale cytoplasm in *Col17a1*-KO, with an absence of mucosal folds and urothelial cell hypertrophy, particularly of umbrella cells, in ureter of *Col17a1*-KO (Supplementary Fig. S8A). To evaluate RP urothelium, a region from the RP junction to the thick portion was examined. WT showed a tendency to increase urothelial cell numbers

1 d after UUO (p = 0.095), but *Col17a1*-KO did not (Fig. 7B, p = 0.082 between WT and *Col17a1*-KO 1d after UUO). In both WT and *Col17a1*-KO, CK14$^+$ urothelial cells predominantly localized from around the thin RP to the junction in the collateral kidney, but numbers decreased after UUO. Moreover, the numbers of CK14$^+$ urothelial cells after UUO were significantly lower in *Col17a1*-KO RP than in WT RP (Supplementary Fig. S8B, Fig. 7C and D). In WT RP after UUO, COL17A1$^+$ urothelial cells co-expressed CD44 and partially localized with CK14$^+$ urothelial cells, although CD44$^+$ urothelial cells were mainly found in *Col17a1*-KO (Fig. 7E).

In terms of epithelium-associated molecules, WT samples showed partially faint ZO-1$^+$ and OCLN$^+$ reactions in RP urothelium after UUO; however, the same reactions in *Col17a1*-KO were relatively abundant at the apical portion compared to in WT (Fig. 7F). Further, ectopic OCLN$^+$ urothelial cells were observed with basal urothelial cells in RP and ureter of *Col17a1*-KO with or without UUO (Fig. 7F, Supplementary Fig. S8C). Importantly, following UUO, numerous CD11b$^+$ cells aggregated beneath RP urothelium at the junction between thin and thick RP in WT, but in *Col17a1*-KO, CD11b$^+$ cells were scattered and exhibited few CXCL2$^+$ reactions (Fig. 7G and H).

DISCUSSION

This study demonstrated that obstructive uropathy disrupted the urine-urothelial barrier in both RP and ureter with ectopic urothelial expression of COL17A1, which is involved in urothelial cell proliferation and local immunoreactivity (Fig. 8). In contrast to urothelium, stratified epithelial cells in the epidermis or cornea are constitutively attached to the basement membrane through COL17A1 as a hemidesmosome component[16]. We discovered that following UUO, the beginning of the thick RP urothelium-expressed COL17A1 as well as FOS/JUN, upstream signaling molecules of COL17A1 in urothelial cells[7]. Both transcription factors, comprising activator protein 1, respond to mechanical stress, bacterial infection, or inflammatory cytokines such as IL-6, and tumor necrosis factor alpha[7,27]. Other studies analyzing murine RP urothelium after UUO or ischemic reperfusion injury reported that fibroblast growth factor receptor 2 (FGFR2) is activated by FGF7[13,28], which is produced in smooth muscle cells and fibroblasts[29–31], leading to urothelial cell proliferation. Further, there are several reports that FGFR2 signaling triggers JUN activation in human hepatocytes and gastric cancer[32,33]. Hence, UUO stimulation including internal pressure in the RP cavity and cytokines from urine might activate the FOS/JUN pathway and subsequently promote COL17A1 expression in urothelial cells.

RP urothelium can be morphologically classified into thin and thick types, which show different characteristics: epithelial layer number, uroplakin expression, microvilli, and fusiform vesicle[23]. Especially, thick RP urothelium with UUO injury possessed multiple layers, as the epithelium in the

433 normal urinary bladder and ureter consists of superficial (including umbrella cells), intermediate, and
434 basal layers. The present study showed that COL17A1^{+} urothelial cells in RP and ureter proliferated and
435 formed several basal layers as shown by IHC and BrdU labeling. COL17A1^{+} urothelial cells partially
436 co-expressed CK14, a progenitor cell marker for urothelial cells[23]. In Sham, CK14^{+} urothelial cells were
437 mainly localized at the basal layer from the RP junction to the thin urothelium, and moderately
438 co-expressed COL17A1, reflecting its function in normal urothelium turnover.
439 At 1 d after UUO, CK14^{+} urothelial cell numbers in RP were lower, while COL17A1^{+} cells
440 increased and partially co-expressed CD44, a glycoprotein involved in cell-cell interaction and cell
441 adhesion, migration, and proliferation in normal urothelium, urothelial carcinoma, and regenerating
442 injured renal epithelium[24,25,34,35]. From 4 d onwards, CK14^{+} urothelial cell numbers increased and some
443 cells co-expressed COL17A1 and CD44, although CK14^{-} COL17A1^{-} CD44^{+} cells were mainly detected
444 in intermediate layers. In *Col17a1*-KO, CK14^{+} urothelial cell numbers decreased in the RP urothelium of
445 both control and UUO kidneys. At 1 d after UUO, urothelium presented CD44^{+} mono- or bilayers.
446 Studies on normal epidermis, wound healing, and epithelial cancers have consistently shown that
447 COL17A1 plays a role in regulating epithelial cell proliferation[2,5,16,25]. There was a loss of progenitor cells
448 and transient hyperproliferation of intrafollicular epidermal cells during pre-maturation in
449 *Col17a1*-KO[5,16,36], as *Col17a1*-KO showed pale cytoplasm and hypertrophy in superficial cells of control
450 RP and ureter, respectively. Our present microarray results reveal upregulation of expression of

451 urothelium-constructing genes, including *Krt14* and *Upk1b*, in the ureter of *Col17a1*-KO 4 d after UUO.
452 It is reported that deficiency of urothelium-associated molecules, such as UPK1B and AT-rich interactive
453 domain-containing protein 1A, eventually induces urothelial hyperproliferation with abnormal
454 morphology[37,38]. Thus, urothelial injury by UUO first induced differentiated urothelial cell proliferation
455 with COL17A1 expression followed by an increase in $CK14^+$ progenitor cell numbers, which would
456 express COL17A1 in a differentiation process (Fig. 8).
457 UUO also altered tight junction protein expression in the urothelium. OCLN was localized at both
458 the apical and basal portions of the urinary tract urothelium, whereas ZO-1 mainly localized at the apical
459 portion, partially consistent with other reports in murine urinary bladder[39]. After UUO, both tight junction
460 proteins were partially absent in urothelial cells at the apical portion of the RP, consistent with decreases
461 in tight junction proteins reported for urinary bladder with interstitial cystitis[40]. However, *Col17a1*-KO 1
462 d after UUO maintained tight junction protein expression at the apical portion of RP urothelium.
463 Moreover, control RP and ureter of *Col17a1*-KO showed predominant expression of OCLN at the basal
464 portion, indicating that COL17A1 deficiency caused abnormal tight junction protein expression.
465 Therefore, COL17A1 may regulate the balance between cell proliferation and differentiation with
466 alteration of cell adhesion in urothelial cells.
467 In RP 1 d after UUO, urine-urothelial barrier disruption at the junction between thin and thick RP
468 urothelium promoted induction of COL17A1 expression. A junction between two organs, such as the

ureteropelvic and the gastroesophageal junctions, can constitute an origin of pathological development[11,41]. In obstruction of the ureteropelvic junction, one crucial pathological mechanism is the presence of abnormalities in synaptic vesicles and smooth muscle cell structure, which can induce alterations in synaptophysin and epidermal growth factor[11]. Interestingly, smooth muscle cells in murine RP are both typical and atypical in that they function as peristaltic contractors and pacemakers, respectively[42]. Thus, atypical and fiber-structural smooth muscle cells that comprise the junction urothelium may lose structural strength in the presence of UUO-induced RP cavity pressure, leading to urine-urothelial barrier disruption and expression of COL17A1.

COL17A1 expressed in mesenchymal progenitor cells of bone marrow influences the regulation of granulocyte production[43]. Our findings supported a COL17A1 function in immunoreactivity; suggesting that COL17A1 is associated with an initial stage of inflammation in urinary tract mucosa through migration of $CD11b^+$ cells secreting CXCL2. CXCL2 is synthesized in macrophages, neutrophils, and mast cells. It is involved in neutrophil recruitment and vascularization as well as skin, intestine, and lung tissue reconstruction[44–46]. This study demonstrated that CXCL2 derived from $CD11b^+$ cells was stimulated by COL17A1 and urine. Ecto- or intra-domains comprising COL17A1 derived from intact or deciduate urothelial cells as well as the ecto-domain in the lamina propria following its shedding may bind to and activate $CD11b^+$ cells[2]; at present the mechanism of action remains unclear. Another immunoactivation process involved urine leakage from the lumen to the parenchyma, which was a factor

promoting UTALS development[7]. In interstitial cystitis, symptoms such as pelvic pain, urgency, and urination frequency are caused by depolarization of sensory nerves and muscles following urinary potassium diffusion into the bladder wall due to an increase in urothelial permeability[40]. We propose that both COL17A1 expression and urine leakage into the parenchyma of the urinary tract may recruit $CD11b^+$ cells leading to CXCL2 production and may contribute to early inflammation and urine-urothelial barrier reconstruction via fibrosis in an attempt to localize the reactions.

One limitation of this study is that findings using *Col17a1*-KO do not show obvious COL17A1 contribution to the progress of hydronephrosis pathology. As shown in Supplementary Fig. S9, the IL-36α^+ renal tubular injury score, but not $CD11b^+$ infiltration cell numbers in tubulointerstitium, deteriorated in *Col17a1*-KO, while $CD11b^+$ cell infiltration into RP was inhibited. The kidneys of *Col17a1*-KO 1 d UUO presented urothelial cell deciduation overlaying renal papilla, suggesting necrosis followed by exacerbation of renal pathology, although further investigations are needed to elucidate COL17A1 function in renal injury induced by UUO. Of note, $COL17A1^+$ $CK14^+$ urothelial cells were found at the beginning of the thin RP in collateral WT kidneys. Reportedly, ischemic reperfusion injury model mice show that Ki-67^+ proliferating urothelial cells, which express CK14, are abundant in this portion (called the fornix area), but not in renal papilla[28]. These findings suggest that urothelial cells localized at the beginning of the thin RP are a potential cell source for RP and papillary urothelium.

We found that ureter urothelium in humans and cats with urolithiasis also overexpressed COL17A1.

505 Previous studies showed upregulation of COL17A1 mRNA expression in human patients with urinary
506 incontinence and canine bladder cancer[47,48]; these findings indicate that COL17A1 could be a common
507 therapeutic target and marker for urothelial disorders in several mammals. Our study also demonstrated
508 that COL17A1 expression in RP and ureter after UUO correlated with urothelial and renal lesions,
509 suggesting that urine-urothelial barrier disruption leads to renal injury. Importantly, RP tissue should not
510 be collected by renal biopsy because of its location. COL17A1 urine could represent a diagnostic marker
511 for both urinary tract and kidney diseases. However, additional research is needed to support this
512 proposal.

513 Overall, this study clarifies a novel pathological pathway involving COL17A1 in the urothelium of
514 mice, humans, and cats with obstructive uropathy. Our data provide a description of a new pathological
515 mechanism through which COL17A1 and urine leakage in urothelium leads to local inflammation. The
516 findings may contribute to the development of therapeutic and diagnostic strategies for urinary organ
517 diseases.

518

519

Author contributions

Ta.N., O.I., and Y.K. designed the study; Ta.N., O.I., K. N., Te.N., and Y.O. performed experiments and analyzed the data; Ta.N., O.I., and Y.K. drafted and revised the manuscript. All authors were involved in the writing of the manuscript and approved the final manuscript.

Acknowledgments

We would like to thank Kazuhisa Oyamada (Matsubara Animal Hospital, Japan), Hazuki Mizukawa (Ehime University, Japan), and Nozomu Yokoyama (Hokkaido University, Japan) for assisting with cat ureter tissue sampling.

REFERENCES

1. Ricard-Blum S. The collagen family: Cold Spring Harb Perspect Biol 2011, 3(1): 1–19.

2. Natsuga K, Watanabe M, Nishie W, Shimizu H: Life before and beyond blistering: The role of collagen XVII in epidermal physiology. Exp Dermatol. 2019, 28(10):1135-1141.

3. Jacków J, Schlosser A, Sormunen R, Nyström A, Sitaru C, Tasanen K, Bruckner-Tuderman L, Franzke CW: Generation of a functional non-shedding collagen XVII mouse model: Relevance of collagen XVII shedding in wound healing. J Inves Dermatol 2016, 136(2):516–525.

4. Jacków J, Löffek S, Nyström A, Bruckner-Tuderman L, Franzke CW: Collagen XVII shedding suppresses ee-epithelialization by directing keratinocyte migration and dampening mTOR signaling. J Inves Dermatol 2016, 136(5):1031–1041.

5. Liu N, Matsumura H, Kato T, Ichinose S, Takada A, Namiki T, Asakawa K, Morinaga H, Mohri Y, Arcangelis AD, Geroges-Labouesse E, Nanba D, Nishimura EK: Stem cell competition orchestrates skin homeostasis and ageing. Nature 2019, 568(7752):344-350.

6. Owaribe K, Kartenbeck J, Stumpp S, Magin TM, Krieg T, Diaz LA, Franke WW: The hemidesmosomal plaque. I. Characterization of a major constituent protein as a differentiation marker for certain forms of epithelia. Differentiation 1990, 45(3):207–220.

7. Ichii O, Hosotani M, Masum A, Horino T, Otani Y, Namba T, Nakamura T, Hosny Ali EY, Kon Y: Close association between altered urine–urothelium barrier and tertiary lymphoid structure

548 formation in the renal pelvis during nephritis. J Am Soc Nephrol 2022, 33(1):88–107.

549 8. Wilson DR, Wilson DDR: Pathophysiology of obstructive nephropathy. Kidney Int 1980,

550 18(3):281–292.

551 9. Washino S, Hosohata K, Miyagawa T: Roles played by biomarkers of kidney injury in patients with

552 upper urinary tract obstruction. Int J Mol Sci 2020, 21(15):1–18.

553 10. Sorokin I, Mamoulakis C, Miyazawa K, Rodgers A, Talati J, Lotan Y: Epidemiology of stone

554 disease across the world. World J Urol 2017, 35(9):1301–1320.

555 11. Hashim H, Woodhouse CRJ: Ureteropelvic junction obstruction. Eur Urol Open Sci 2012,

556 11(2):25–32.

557 12. Kawaguchi S: The ultrastructural changes of experimental hydroureter in rats. Jpn J Urol 1981,

558 72(11):1399–1412.

559 13. Girshovich A, Vinsonneau C, Perez J, Vandermeersch S, Verpont MC, Placier S, Jouanneau C,

560 Letavernier E, Baud L, Haymann JP: Ureteral obstruction promotes proliferation and differentiation

561 of the renal urothelium into a bladder-like phenotype. Kidney Int 2012, 82(4):428–435.

562 14. Nishie W, Sawamura D, Goto M, Ito K, Shibaki A, McMillan JR, Sakai K, Nakamura H, Olasz E,

563 Yancey KB, Akiyama M, Shimizu H: Humanization of autoantigen. Nat Med 2007, 13(3):378–383.

564 15. Nishie W, Sawamura D, Natsuga K, Shinkuma S, Goto M, Shibaki A, Ujiie H, Olasz E, Yancey KB,

565 Shimizu H: A novel humanized neonatal autoimmune blistering skin disease model induced by

maternally transferred antibodies. J Immunol 2009, 183(6):4088–4093.

16. Watanabe M, Natsuga K, Nishie W, Kobayashi Y, Donati G, Suzuki S, Fujimura Y, Tsukiyama T, Ujiie H, Shinkuma S, Nakamura H, Murakami M, Ozaki M, Nagayama M, Watt FM, Shimizu H:Type XVII collagen coordinates proliferation in the interfollicular epidermis. Elife 2017, 6:e26635.

17. Fujimura Y, Watanabe M, Ohno K, Kobayashi Y, Takashima S, Nakamura H, Kosumi H, Wang Y, Mai Y, Lauria A, Proserpio V, Ujiie H, Iwata H, Nishie W, Nagayama M, Oliviero S, Donati G, Shimizu H, Natsuga K: Hair follicle stem cell progeny heal blisters while pausing skin development. EMBO Rep 2021, 22(7): e50882.

18. Namba T, Ichii O, Nakamura T, Masum MA, Otani Y, Hosotani M, Ali Elewa YH, Kon Y: Compartmentalization of interleukin 36 subfamily according to inducible and constitutive expression in the kidneys of a murine autoimmune nephritis model. Cell Tissue Res 2021, 386(1):59–77.

19. Fujiu K, Manabe I, Nagai R: Renal collecting duct epithelial cells regulate inflammation in tubulointerstitial damage in mice. J Clin Invest 2011, 121(9):3425–3441.

20. Ichii O, Kimura J, Okamura T, Horino T, Nakamura T, Sasaki H, Ali Elewa YH, Kon Y: IL-36α Regulates tubulointerstitial inflammation in the mouse kidney. Front Immunol 2017, 8:1346.

21. Dru Forrester S, Roudebush P: Evidence-based management of feline lower urinary tract disease.

584 Vet Clin North Am Small Anim Pract 2007, 37(3):533–558.

585 22. Ichii O, Oyamada K, Mizukawa H, Yokoyama N, Namba T, Otani Y, Ali Elewa YH, Sasaki N,

586 Nakmura T, Kon Y: Ureteral morphology and pathology during urolithiasis in cats. Res Vet Sci 2022,

587 10;151:10–20.

588 23. Romih R, Korosec P, Mello Jr WD, Jezernik K: Differentiation of epithelial cells in the urinary tract.

589 Cell Tissue Res 2005, 320(2):259-268.

590 24. Ho PL, Kurtova A, Chan KS: Normal and neoplastic urothelial stem cells: getting to the root of the

591 problem. Nat Rev Urol 2012, 9(10):583–594.

592 25. Denning SM, Le PT, Singer KH, Haynes BF: Antibodies against the CD44 p80, lymphocyte homing

593 receptor molecule augment human peripheral blood T cell activation. J Immunol 1990, 144(1):7–15.

594 26. Kozawa K, Sekai M, Ohba K, Ito S, Sako H, Maruyama T et al.: The CD44/COL17A1 pathway

595 promotes the formation of multilayered, transformed epithelia. Curr Biol 2021,

596 31(14):3086-3097.e7.

597 27. McKay S, Bromhaar MMG, de Jongste JC, Hoogsteden HC, Saxena PR, Sharma HS:

598 Pro-inflammatory cytokines induce c-fos expression followed by IL-6 release in human airway

599 smooth muscle cells. Mediators Inflamm 2001, 10(3):135–142.

600 28. Vinsonneau C, Girshovich A, Ben M'Rad M, Perez J, Mesnard L, Vandermersch S, Placier S,

601 Letavernier E, Baud L, Haymann JP: Intrarenal urothelium proliferation: An unexpected early event

following ischemic injury. Am J Physiol Renal Physiol 2010, 299(3):479–486.

29. El Agha E, Schwind F, Ruppert C, Günther A, Bellusci S, Schermuly RT, Kosanovic D: Is the fibroblast growth factor signaling pathway a victim of receptor tyrosine kinase inhibition in pulmonary parenchymal and vascular remodeling? Am J Physiol Lung Cell Mol Physiol 2018, 315(2):L248–L252.

30. Peng Y, Wu S, Tang Q, Li S, Peng C: KGF-1 accelerates wound contraction through the TGF-β1/Smad signaling pathway in a double-paracrine manner. J Biol Chem 2019, 294(21):8361–8370.

31. Cheng X, Lai H, Luo W, Zhang M, Miao J, Song W, Xing S, Wang J, Gao WQ: Single-cell analysis reveals urothelial cell heterogeneity and regenerative cues following cyclophosphamide-induced bladder injury. Cell Death Dis 2021, 12(5):446.

32. Zhang J, Wong CC, Leung KT, Wu F, Zhou Y, Tong JHM, Chan RCK, Li H, Wang Y, Yan H, Liu L, Wu WKK, Chan MWY, Cheng ASL, Yu J, Wong N, Lo KW, To KF, Kang W: FGF18–FGFR2 signaling triggers the activation of c-Jun–YAP1 axis to promote carcinogenesis in a subgroup of gastric cancer patients and indicates translational potential. Oncogene 2020, 39(43):6647–6663.

33. Sato-Matsubara M, Matsubara T, Daikoku A, Okina Y, Longato L, Rombouts K, Thuy LTT, Adachi J, Tomonaga T, Ikeda K, Yoshizato K, Pinzani M, Kawada N: Fibroblast growth factor 2 (FGF2) regulates cytoglobin expression and activation of human hepatic stellate cells via JNK signaling. J

Biol Chem 2017, 292(46):18961–18972.

34. Eng DG, Sunseri MW, Kaverina N V., Roeder SS, Pippin JW, Shankland SJ: Glomerular parietal epithelial cells contribute to adult podocyte regeneration in experimental focal segmental glomerulosclerosis. Kidney Int 2015, 88(5):999–1012.

35. Lewington AJP, Padanilam BJ, Martin DR, Hammerman MR: Expression of CD44 in kidney after acute ischemic injury in rats. Am J Physiol Regul Integr Comp Physiol 2000, 278(1):R247–R254.

36. Tanimura S, Tadokoro Y, Inomata K, Binh NT, Nishie W, Yamazaki S, Nakauchi H, Tanaka Y, McMillan JR, Sawamura D, Yancey K, Shimizu H, Nishimura EK: Hair follicle stem cells provide a functional niche for melanocyte stem cells. Cell Stem Cell 2011, 8(2):177–187.

37. Guo C, Zhang Y, Tan R, Tang Z, Lam CM, Ye X, Wang Z, Li X: Arid1a regulates bladder urothelium formation and maintenance. Dev Biol 2022, 485:61–69.

38. Carpenter AR, Becknell MB, Ching CB, Cuaresma EJ, Chen X, Hains DS, McHugh KM: Uroplakin 1b is critical in urinary tract development and urothelial differentiation and homeostasis. Kidney Int 2016, 89(3):612–624.

39. Acharya P, Beckel J, Ruiz WG, Wang E, Rojas R, Birder L, Apodaca G: Distribution of the tight junction proteins ZO-1, occludin, and claudin-4, -8, and -12 in bladder epithelium. Am J Physiol Renal Physiol 2004, 287(2):F305–F318.

40. Lee JD, Lee MH: Decreased expression of zonula occludens-1 and occludin in the bladder

638 urothelium of patients with interstitial cystitis/painful bladder syndrome. J Formos Med Assoc 2014,
639 113(1):17–22.
640 41. Buas MF, Vaughan TL: Epidemiology and risk factors for gastroesophageal junction tumors:
641 understanding the rising incidence of this disease. Semin Radiat Oncol 2013, 23(1):3–9.
642 42. Grainger N, Freeman RS, Shonnard CC, Drumm BT, Koh SD, Ward SM, Sanders KM:
643 Identification and classification of interstitial cells in the mouse renal pelvis. J Physiol 2020,
644 598(15):3283–3307.
645 43. Lin L, Hwang BJ, Li N, Googe P, Diaz LA, Miao E, Vilen B, Thomas NE, Ting J, Liu Z:
646 Non-cell-autonomous activity of the hemidesmosomal protein BP180/collagen XVII in
647 granulopoiesis in humanized NC16A mice. J Immunol 2020, 205(10):2786–2794.
648 44. De Filippo K, Dudeck A, Hasenberg M, Nye E, Van Rooijen N, Hartmann K, Gunzer M, Roers A,
649 Hogg N: Mast cell and macrophage chemokines CXCL1/CXCL2 control the early stage of
650 neutrophil recruitment during tissue inflammation. Blood 2013, 121(24):4930–4937.
651 45. Esser-von Bieren J, Volpe B, Sutherland DB, Bürgi J, Verbeek JS, Marsland BJ, Urban Jr JF, Harris
652 NL: Immune antibodies and helminth products drive CXCR2-dependent macrophage-myofibroblast
653 crosstalk to promote intestinal repair. PLoS Pathog 2015, 11(3):1–23.
654 46. Al-Alwan LA, Chang Y, Mogas A, Halayko AJ, Baglole CJ, Martin JG, Rousseau S, Eidelman DH,
655 Hamid Q: Differential roles of CXCL2 and CXCL3 and their receptors in regulating normal and

asthmatic airway smooth muscle cell migration. J Immunol 2013, 191(5):2731–2741.

47. Isali I, Mahran A, Khalifa AO, Sheyn D, Neudecker M, Qureshi A, Conroy B, Schumacher FR, Hijaz AK, El-Nashar SA: Gene expression in stress urinary incontinence: a systematic review. Int Urogynecol J 2020, 31(1):1–14.

48. Elbadawy M, Usui T, Mori T, Tsunedomi R, Hazama S, Nabeta R, Uchide T, Fukushima R, Yoshida T, Shibutani M, Tanaka T, Masuda S, Okada R, Ichikawa R, Omatsu T, Mizutani T, Katayama Y, Noguchi S, Iwai S, Nakagawa T, Shinohara Y, Kaneda M, Yamawaki H, Sasaki K: Establishment of a novel experimental model for muscle-invasive bladder cancer using a dog bladder cancer organoid culture. Cancer Sci 2019, 110(9):2806–2821.

666 **Table 1. Antibodies used in this study**

	Antibody	Cat. No.	Host	Dilution	Source	Antigen retrieval	Blocking serum	
							IHC	IF
Primary antibodies	α-SMA	ab5694	Rabbit	1:3000	Abcam, Cambridge, UK	Tris	10% NGS	-
	α-SMA	67735-1lg	Mouse	1:8000	Proteintech, Rosemont, IL, USA	Tris	-	5% NDS
	B220	CLB8990AP	Rat	1:1600	Cedarlane, Burlington, Canada	Tris	10% NGS	-
	CD11b	ab133357	Rabbit	1:5000	Abcam, Cambridge, UK	Tris	10% NGS	5% NDS
	CD3	F1709	Rabbit	1:200	Nichirei, Tokyo, Japan	Tris	10% NGS	-
	CD44	553131	Rat	1:800	BD Biosciences, San Jose, CA, USA	Tris		5% NDS
	COL17A1	ab184996	Rabbit	1:100	Abcam, Cambridge, UK	Tris	10% NGS	5% NDS
	CXCL2	AF-452	Goat	1:400	R&D Systems, Minneapolis, MN, USA	Tris	-	5% NDS
	CK14	60320-1-Ig	Mouse	1:500	Proteintech, Rosemont, IL, USA	Tris	Mouse kit*	5% NDS
	c-FOS	ab222699	Rabbit	1:400	Abcam, Cambridge, UK	Tris	10% NGS	-
	c-JUN	ab40766	Rabbit	1:400	Abcam, Cambridge, UK	Tris	10% NGS	-
	Gr-1	MAB1037	Rat	1:800	R&D Systems, Minneapolis, MN, USA	Pepsin	10% NGS	-
	IBA-1	ab48004	Goat	1:600	Abcam, Cambridge, UK	Tris	-	5% NDS
	IL-36α	AF2297	Goat	1:400	R&D Systems, Minneapolis, MN, USA	CB	5% NDS	-
	OCLN	66378-1	Mouse	1:1000	Proteintech, Rosemont, IL, USA	Pepsin	-	5% NDS
	PDGFRα	AF1062	Goat	1:300	R&D Systems, Minneapolis, MN, USA	Tris	-	5% NDS
	ZO-1	ab221547	Rabbit	1:1000	Abcam, Cambridge, UK	Pepsin	-	5% NDS
Secondary antibodies	Rat IgG-biotin	405428	Donkey	1:400	Biolegend, San Diego, CA, USA			
	Rabbit IgG-biotin	426012	Donkey	Undiluted	SABPO(R)Kit; Nichirei, Tokyo, Japan			

	Goat IgG-biotin	ab6884	Donkey	1:200	Abcam, Cambridge, UK	
	Rabbit IgG-Alexa Fluor 488	A21206	Donkey	1:500	Thermo Fisher Scientific, Waltham, MA, USA	
	Rabbit IgG-Alexa Fluor 546	A10040	Donkey	1:500	Thermo Fisher Scientific, Waltham, MA, USA	
	Rat IgG-Alexa Fluor 488	A21208	Donkey	1:500	Thermo Fisher Scientific, Waltham, MA, USA	
	Rat IgG-Alexa Fluor 594	A21209	Donkey	1:500	Thermo Fisher Scientific, Waltham, MA, USA	
	Goat IgG-Alexa Fluor 546	A11056	Donkey	1:500	Thermo Fisher Scientific, Waltham, MA, USA	
	Goat IgG-Alexa Fluor 647	A21447	Donkey	1:500	Thermo Fisher Scientific, Waltham, MA, USA	
	Mouse IgG-Alexa Fluor 546	A10036	Donkey	1:500	Thermo Fisher Scientific, Waltham, MA, USA	

667 Tris: 20 mM Tris-HCl buffer (pH 9.0) at 110 °C for 15 min; CB: 10 mM citrate buffer (pH 9.0) at 110 °C for 15 min; Pepsin: 0.1% pepsin at 37 °C for 5
668 min; NDS: normal donkey serum; NGS: normal goat serum; *: N-histofine® Mouse stain Kit (Nichirei, Tokyo, Japan).

669 **Table 2. Primers used in this study**

Gene symbol (Gene ID)	Primer sequence F: Forward, R: Reverse		Product size (bp)
Actb (11461)	F: 5′-TGTTACCAACTGGGACGACA-3′	R: 5′-GGGGTGTTGAAGGTCTCAAA-3′	165
Cd3e (12501)	F: 5′-TGCCTCAGAAGCATGATAAGC-3′	R: 5′-TTGGCCTTCCTATTCTTGCTC-3′	244
Col17a1 (12821)	F: 5′-ACTTGCGGTCATCAGGCTAC-3′	R: 5′-AGACAGGAGGGACCCATCTC-3′	170
Ccl1 (20290)	F: 5′-GCAAGAGCATGCTTACGGTC-3′	R: 5′-TTTGTTAGTTGAGGCGAGC-3′	170
Ccl6 (20305)	F: 5′-CAGGAGGATGAGAAACTCCAA-3′	R: 5′-TTGGAGGGTTATAGCGACGA-3′	119
Ccl25 (20300)	F: 5′-AGTGGAAGCTGCAACCTACG-3′	R: 5′-CCTCACGCTTGTACTGTTGG-3′	216
Cxcl2 (20310)	F: 5′-TGTCAATGCCTGAAGACCCTG-3′	R: 5′-CAGTTAGCCTTGCCTTTGTTCAG-3′	197
Cxcl10 (15945)	F: 5′-ATGACGGGCCAGTGAGAATG-3′	R: 5′-CGGATTCAGACATCTCTGCTCAT-3′	125
Cxcl11 (56066)	F: 5′-AGTAACGGCTGCGACAAAG-3′	R: 5′-AGACGTTCCCAGGATGTCAC -3′	160
Cxcl12 (20315)	F: 5′-CTTCGAGAGCCACATCGCC-3′	R: 5′-GTTGTTGTTCTTCAGCCGTGC-3′	100
Cxcl13 (55985)	F: 5′-ATCCTCGTGCAAATGGTTACA-3′	R: 5′-AGATGATAGTGGCTTCAGGCAG-3′	115
Ifng (15978)	F: 5′-CCTTTGGACCCTCTGACTTG-3′	R: 5′-TTCCACATCTATGCCACTTGAG-3′	201
Il1b (16176)	F: 5′-TTCCAGGATGAGGACATGAGC-3′	R: 5′-AATGGGACGTCACACACCAG-3′	110
Il6 (16193)	F: 5′-CAACGATGATGCACTTGCAGA-3′	R: 5′-GGTACTCCAGAAGACCAGAGGA-3′	112
Ms4a1 (12482)	F: 5′-ATCATGAATGGCCTCTTCCA-3′	R: 5′-TGCCAGGAGTGATCCTGAA-3′	138
Ocln (18260)	F: 5′-TCCACCTCCTTACAGACCTGA-3′	R: 5′-AGAGTACGCTGGCTGAGAGA-3′	112
Tgfb1 (21803)	F: 5′-ATGCTAAAGAGGTCACCCGC-3′	R: 5′-TGCTTCCCGAATGTCTGACG-3′	119
Tjp1 (21872)	F: 5′-AATTATCCCACAAGGAGCCATTCC-3′	R: 5′-TTTAGGGTCACAGTGTGGCAA-3′	196
Tnf (21926)	F: 5′-TCTTCTCATTCCTGCTTGTGGC-3′	R: 5′-CATAGAACTGATGAGAGGGAGGC-3′	119
Upk2 (22269)	F: 5′-AAGCCTGTTAATTGCCTTGCC-3′	R: 5′-CATGGAGGCACCACAAAGTC-3′	114
Col17a1 (wild type)	F: 5′-ACCTTCCAGTGAAGAGCCAT-3′	R: 5′-GTGGATTCCCAAAGCCATAC-3′	533
Col17a1 (knockout type)	F: 5′-TGGATGTGGAATGTGTGCGA-3′	R: 5′-GTGGATTCCCAAAGCCATAC-3′	590

Table 3. Relative mRNA expression of chemokines in mouse lymphoid structures stimulated by urine

Gene	Fold
Cxcl2	4.49
Cxcl11	4.16
Cxcl12	3.71
Cxcl10	3.67
Ccl6	3.02
Cxcl13	2.82
Ccl1	2.48
Ccl25	2.30

Expression levels are normalized to the values of the PBS control and determined using microarrays.

Table 4. Gene Ontology (GO) of the ureter in *Col17a1*-KO 4 d after unilateral ureteral obstruction (UUO)

Gene	Pathway GO ID	Pathway description	Gene count	FDR
Upregulated genes	0009617	Response to bacterium	19	2.2×10^{-3}
	0070269	Pyroptosis	5	4.7×10^{-3}
	0060429	Epithelium development	23	4.7×10^{-3}
	0009888	Tissue development	30	4.7×10^{-3}
	0009605	Response to external stimulus	35	4.7×10^{-3}
	0050896	Response to stimulus	76	4.7×10^{-3}
	0051707	Response to other organism	22	2.3×10^{-3}
	0030855	Epithelial cell differentiation	14	3.1×10^{-2}
	0044419	Interspecies interaction between organisms	23	3.6×10^{-2}
	0048856	Anatomical structure development	58	4.1×10^{-2}
Downregulated genes	0002682	Regulation of immune system process	34	1.3×10^{-7}
	0002376	Immune system process	40	5.8×10^{-7}
	0002694	Regulation of leukocyte activation	20	6.2×10^{-6}
	0044419	Interspecies interaction between organisms	31	7.9×10^{-6}
	0050896	Response to stimulus	84	7.9×10^{-6}
	0051707	Response to other organism	28	1.6×10^{-5}
	0031638	Zymogen activation	8	2.0×10^{-5}
	0045321	Leukocyte activation	18	3.2×10^{-5}
	0006955	Immune response	25	3.2×10^{-5}
	0006952	Defense response	27	3.2×10^{-5}

Ten GO terms each are listed for genes with up- or downregulated expression in the ureter of *Col17a1*-knockout mice 4 d after UUO, compared with the wild-type. Gene Ontology Resource (https://geneontology.org/) was used for Gene Ontology (GO) analysis. FDR: false discovery rate.

FIGURE LEGENDS

Fig. 1 Collagen 17A1 (COL17A1) expression in human and cat ureter with and without urolithiasis

(A) Representative images of human and cat ureter. More collagen fibers are observed in diseased human and feline ureters than in normal ureters. Infiltrating cells localize in the lamina propria and submucosa of humans and cats with urolithiasis. In the human specimen, immune cell aggregation is observed (arrow). Masson's trichrome staining. Bars = 100 μm.

(B) Localization of COL17A1 in human ureter. Few $COL17A1^+$ cells are observed in the basal portion of normal ureter urothelia. There are numerous $COL17A1^+$ cells in diseased ureter with cell aggregation. Each inset indicates a highly magnified image of the area marked by a black dashed square. Immunohistochemistry. Bars = 100 μm.

(C) Localization of *COL17A1* in cat ureter. $COL17A1^+$ reactions are observed at the basal portion of both normal and diseased ureter. Positive-reaction dots in cells are abundant in diseased ureters. Each inset indicates a highly magnified image of the area marked by a black dashed square. *In situ* hybridization. Bars = 100 μm.

Fig. 2 Collagen 17A1 (COL17A1) expression in the urothelium of murine ureter induced by unilateral ureteral obstruction (UUO)

(A) Localization of COL17A1 in ureter at 1, 4, and 7 d after UUO compared to in sham-operation (Sham). $COL17A1^+$ urothelial cells are not detected in the Sham ureter. $COL17A1^+$ urothelial cells are observed in basal ureter 1 d after UUO and increase substantially from 4 d. Each inset indicates a highly magnified image of the area marked by a black dashed square. Immunohistochemistry. Bars = 500 μm.

(B) $COL17A1^+$ area in ureter urothelium. Each bar represents mean ± SE (n = 5). **, ††, ##, and §§ indicate a significant difference to Sham, 1, 4, and 7 d after UUO, respectively ($P < 0.01$). The Kruskal-Wallis test was used followed by Scheffé's method. ND, not detected.

(C) Correlation of $COL17A1^+$ area in ureter urothelium with the luminal size of the ureter (Ur) and indices of renal lesions including $CD11b^+$ cells in tubulointerstitium (Ti) and IL-$36\alpha^+$ injured renal tubules. ρ indicates Spearman's correlation coefficient (n = 20, $P < 0.01$).

(D) Representative images of ureter 1 and 4 d after UUO. Deciduation of urothelial cells (arrow) is seen with mononuclear cells at 4 d but not 1 d after UUO. Inset indicates a highly magnified image of the area marked by a black dashed square. Periodic acid Schiff and hematoxylin staining (PAS-H). Bars = 100 μm.

(E) Relative mRNA expression of epithelium-associated genes in the ureter at 7 d after UUO. Expression levels are normalized to those of β-actin and the collateral control (Cont). Each bar represents mean ± SE (n = 4–5). * indicates a significant difference compared to the Cont (*$P < 0.05$, ** $P < 0.01$). The Mann–Whitney *U*-test and quantitative PCR analysis were used.

(F) Localization of ZO-1 (green) and OCLN (red) in ureter at 1, 4, and 7 d after UUO compared with

Sham. ZO-1^+ and $OCLN^+$ staining in Sham urothelium are seen at the apical and apical/basal portions, respectively. ZO-1^+ staining is faint after UUO. Although $OCLN^+$ staining is also faint in the apical portion 1 d after UUO, it increases temporarily 4 d after UUO, and subsequently OCLN-overexpressing and -faint urothelial cells are observed 7 d after UUO. The nucleus was stained using Hoechst (blue). Each inset indicates a highly magnified image of the area marked by a white dashed square. Immunofluorescence. Bars = 100 μm.

(G) Localization of COL17A1 (green) using bromodeoxyuridine (BrdU; red) in ureter at 7 d after UUO. Some BrdU-incorporated cells express COL17A1 (arrowheads), whereas COL17A1 urothelial cells incorporating BrdU (arrows) are also found on the apical side of the urothelium. White dotted lines represent the apical side of the urothelium. The nucleus was stained using Hoechst (blue). Immunofluorescence. Bars = 50 μm.

Fig. 3 Upregulation of chemokine expression in immune cells stimulated by urine or COL17A1 and in ureter with UUO

(A) Relative mRNA expression of chemokines in the ureter determined 7 d after UUO. The expression levels are normalized to those of β-actin and the collateral control (Cont). Each bar represents mean ± SE (n = 5). * indicates a significant difference compared to Cont (*$P < 0.05$, **$P < 0.01$). The Mann–Whitney *U*-test and quantitative PCR analysis were used.

(B) Relative mRNA expression of *Cxcl2* in B, T, and $CD11b^+$ cells stimulated using bovine serum albumin (BSA) or recombinant human COL17A1. The expression levels are normalized to those of β-actin and B cells stimulated with BSA. Each bar represents the mean ± SE (n = 4). * indicates a significant difference compared with the BSA-stimulated group (*$P < 0.05$). The Mann–Whitney *U*-test and quantitative PCR analysis were used.

(C) Localization of CXCL2 (red) with ZO-1, COL17A1, or CD11b (green) in the ureter at 7 d after UUO. $CXCL2^+$ staining is observed beneath the ZO-1 faint urothelium as well as close to the $COL17A1^+$ urothelium and is localized in $CD11b^+$ cells. White dotted lines represent the apical side of the urothelium. Each inset indicates a highly magnified image of the area marked by a white dashed square. The nucleus was stained using Hoechst (blue). Immunofluorescence. Bars = 100 μm.

(D) Relative mRNA expression of inflammatory cytokines measured in ureter 7 d after UUO. The expression levels are normalized to those of β-actin and Cont. Each bar represents the mean ± SE (n = 4–5). * indicates a significant difference compared with Cont (*$P < 0.05$, **$P < 0.01$). The Mann–Whitney *U*-test and quantitative PCR analysis were used.

Fig. 4 COL17A1 dynamics in mouse renal pelvis (RP) after UUO

(A) Localization of α-SMA in the Sham RP. There is no $\alpha\text{-SMA}^+$ smooth muscle layer in the thin RP urothelium covering the inner stripe of the outer medulla (IOM; panel A'). At the junction between the

753 thin and thick RP urothelium on the outer stripe of the outer medulla (OOM), α-SMA$^+$ cells exhibit a fiber

754 structure, not a smooth muscle layer (panel A''). A smooth muscle layer is observed in the thick RP

755 urothelium covering cortex (Co; panel A'''). Arrows indicate the junction between the thin and thick RP.

756 IM, inner medulla. Immunohistochemistry. Bars = 1 mm (A) and 50 μm (A'-A''').

757 **(B)** Localization of COL17A1 in RP 1, 4, and 7 d after UUO compared to in Sham. COL17A1$^+$ urothelial

758 cells localize at the basal portion of RP urothelium and substantially increase in a time-dependent manner

759 after UUO. Each inset indicates a highly magnified image of the area marked by a black dashed square.

760 Arrows indicate the junction between the thin and thick RP. Immunohistochemistry. Bars = 100 μm.

761 **(C)** Co-localization of COL17A1 (white) with PDGFRα (green, fibroblast marker) and α-SMA (red,

762 smooth muscle fiber and myofibroblast marker) in RP at 1, 4, and 7 d after UUO compared with in Sham.

763 RP urothelium in Sham is divided into thin RP urothelium without the α-SMA$^+$ smooth muscle layer and

764 thick urothelium with the smooth muscle layer, where the latter contains COL17A1$^+$ cells at 1 d UUO.

765 COL17A1$^+$ cells increase in both types of urothelium with αSMA$^+$ myofibroblasts increasing from 4 d

766 after UUO. The nucleus is stained using Hoechst (blue). Arrow indicates deciduation of urothelial cells.

767 White dotted lines represent the apical side of the urothelium. Immunofluorescence. Bars = 100 μm.

768 **(D)** Relative mRNA expression of *Col17a1* in isolated RP and ureter 1 d after UUO. The expression

769 levels are normalized to those of β-actin and the collateral control (Cont). Each bar represents the mean ±

770 SE (n = 4–5). * indicates a significant difference between groups (*$P < 0.05$). The Mann–Whitney *U*-test

771 and quantitative PCR analysis were used.

772 **(E)** Consecutive length of CO17A1^{+} urothelial cells from the RP junction to the thin and thick parts 1 d

773 after UUO. Each bar represents the mean ± SE (n = 5). * indicates a significant difference between groups

774 (*$P < 0.05$). Mann–Whitney *U*-test.

775 **(F)** COL17A1^{+} area in the thin and thick RP urothelium. Each bar represents mean ± SE (n = 5). **, ††,

776 ##, and §§ indicate a significant difference compared to that in Sham, 1, 4, and 7 d, respectively ($P <$

777 0.01). The Kruskal–Wallis test was used followed by Scheffé's method.

778 **(G)** Correlation of COL17A1^{+} area in thin or thick RP urothelium with indices for renal lesions, CD11b^{+}

779 cells in tubulointerstitium (Ti) and IL-36α^{+} renal tubules. ρ indicates Spearman's correlation coefficient (n

780 = 20, $P < 0.01$).

781 **(H)** Localization of FOS and JUN in RP. Both FOS and JUN positive reactions are observed in urothelial

782 nuclei at the beginning of the thick urothelium 1 d after UUO, but not in Sham urothelium. Each inset

783 indicates a highly magnified image of the area marked by a black dashed square. Arrows indicate the

784 junction between the thin and thick RP. Immunohistochemistry. Bars = 100 μm.

785

786 **Fig. 5 Disruption of the urine-urothelial barrier in murine RP with UUO**

787 **(A)** Representative images of RP 1 d after UUO. Although intact urothelium of RP is observed in Sham,

788 deciduation of urothelial cells is observed at the junction between the thin and thick urothelium 1 d after

789 UUO (arrow). PAS-H. Bars = 100 μm.

790 **(B)** Relative mRNA expression of epithelium-associated genes in isolated RPs at 1 d after UUO. The

791 expression levels are normalized to those of β-actin and Cont. Each bar represents mean ± SE (n = 4–5). *

792 indicates a significant difference compared with Cont (*P< 0.05). The Mann–Whitney U-test and

793 quantitative PCR analysis were used.

794 **(C)** Localization of ZO-1 (green) and OCLN (red), as markers for tight junctions in RP at 1, 4, and 7 d

795 after UUO compared with those in Sham. ZO-1^{+} and OCLN^{+} staining are observed at the apical and

796 apical/basal portions of RP urothelium, respectively in Sham. Both positive reactions are partially faint at

797 the apical portion on day 1 after UUO with urothelial deciduation (arrow). OCLN-faint and

798 -overexpressing urothelial cells are observed 4 d after UUO. The former cell type increases 7 d after UUO.

799 The nucleus was stained using Hoechst (blue). White dotted lines represent the apical side of the

800 urothelium. Each inset indicates a highly magnified image of the area marked by a white dashed square.

801 Immunofluorescence. Bars = 100 μm.

802 **(D)** Localization of COL17A1 (green) with CD44 (red) and CK14 (white) in RP at 1, 4, and 7 d after

803 UUO compared with in Sham. In Sham, COL17A1^{-} CD44^{-} CK14^{+} cells (white arrowheads) are found and

804 partially co-expressed with COL17A1 (yellow arrowheads). At 1 d, COL17A1^{+} CD44^{+} CK14^{-} cells

805 (yellow arrows) are dominant, and few COL17A1^{+} CD44^{+} CK14^{+} cells (white arrows) are observed.

806 From 4 d onwards, triple-positive cells are dominant, and some COL17A1^{-} CD44^{+} CK14^{-} cells are seen

(red arrowheads). The nucleus was stained using Hoechst (blue). White dotted lines represent the apical side of the urothelium. Each inset indicates a highly magnified image of the area marked by a white dashed square. Immunofluorescence. Bars = 50 μm.

(E) Representative transmission electron microscopy images of RP. In urothelial cells 1 d after UUO, folded apical membrane (white arrows), numerous lysosomes (black arrows), ectopic red blood cells beneath basement membrane (white asterisks), and intracellular spaces (black asterisks) are observed, distinct from those in Cont. Urothelial cell processes extending to the lamina propria interact with smooth muscle cells (white arrowheads). A migrating cell from lamina propria is observed in the partially effaced basement membrane (black arrowheads). UC, urothelial cell; MC, migrating cell; BM, basement membrane. Bars = 2 μm.

(F) Localization of Evans blue conjugated with bovine serum albumin (EBA) in RP. EBA injected from the urinary bladder is observed along the urothelium in the Sham group, where it leaked into RP parenchyma (Pa) from the lumen (Lu) 1 d after UUO (asterisks). Bars = 100 μm.

Fig. 6 Activation of $CXCL2^+$ $CD11b^+$ cells in murine RP 1 d after UUO

(A) Relative mRNA expression of *Cxcl2* measured from isolated RP 1 d after UUO. The expression levels are normalized to the values of β-actin and collateral control (Cont). Each bar represents mean ± SE (n = 4–5). * indicates a significant difference compared with Cont (*$P < 0.05$). The Mann–Whitney *U*-test and

825 quantitative PCR analysis were used.

826 **(B)** Localization of ZO-1 (green) and CXCL2 (red) in RP. $CXCL2^+$ staining is observed beneath

827 ZO-1-deficient urothelium (arrows) at the junction between thin and thick RP urothelium 1 d after UUO

828 or at thin urothelium 7 d after UUO. The nucleus was stained using Hoechst (blue). White dotted lines

829 represent the apical side of the urothelium. Lu, RP lumen; IM, inner medulla. Immunofluorescence. Bars

830 = 100 μm.

831 **(C)** Relative mRNA expression of immune cell genes in RP 1 d after UUO. The expression levels are

832 normalized to those of β-actin and Cont. Each bar represents mean ± SE (n = 4–5). * indicates a

833 significant difference compared to Cont (*$P < 0.05$). Mann–Whitney *U*-test and quantitative PCR analysis

834 were used.

835 **(D)** Localization of $CD11b^+$ cells in RP. There are few $CD11b^+$ cells in Sham, and the number increases

836 from 1 d after UUO, then decreases 4 d after UUO. Immunohistochemistry. Bars = 100 μm.

837 **(E)** Localization of CXCL2 (red) with CD11b or COL17A1 (green) in RP. $CXCL2^+$ staining is observed

838 in $CD11b^+$ cells beneath the $COL17A1^+$ urothelium 1 d after UUO. The nucleus was stained using

839 Hoechst (blue). White dotted lines indicate the apical side of the urothelium. The arrow indicates

840 deciduation of urothelial cells. Immunofluorescence. Bars = 100 μm.

841 **(F)** Relative mRNA expression of inflammatory cytokines measured in isolated RPs 1 d after UUO. The

842 expression levels are normalized to those of β-actin and Cont. Each bar represents the mean ± SE (n =

4–5). * indicates a significant difference compared with Cont (*$P < 0.05$). The Mann–Whitney *U*-test and quantitative PCR analysis were used.

Fig. 7 Altered pathology of RP urothelium in *Col17a1*-KO mice 1 d after UUO

(A) Representative images of RP from *Col17a1*-KO and wild-type (WT) 1 d after UUO. Deciduation of urothelial cells (arrows) is observed equally in WT and *Col17a1*-KO kidneys. Cell infiltration is more frequently observed in *Col17a1*-KO compared to WT RP. PAS-H. Bars = 50 μm.

(B) Number of urothelial cells in thick RP. Each bar represents mean ± SE (n = 5–6). The Mann–Whitney *U*-test was used.

(C) Localization of cytokeratin 14 (CK14) in RP 1 d after UUO. $CK14^+$ urothelial cells (arrowheads) are observed in both WT and *Col17a1*-KO RP, whereby the numbers are lower in *Col17a1*-KO than in WT RP. Bars = 50 μm.

(D) Number of $CK14^+$ urothelial cells in thick RP. Each bar represents mean ± SE (n = 5–6). * indicates a significant difference compared with Cont (*$P < 0.05$). # indicates a significant difference between Cont and UUO 1 d (# $P < 0.05$). The Mann–Whitney *U*-test was used.

(E) Localization of COL17A1 (green) with CD44 (red) and CK14 (white) in RP 1 d after UUO. $COL17A1^+$ urothelium co-localizing with CD44 (yellow arrows) partially forms multiple layers and co-expresses with CK14 (yellow arrowheads) in WT, whereas $COL17A1^-$ $CD44^-$ $CK14^+$ urothelial cell

numbers are observed to be lower (white arrowhead). $CD44^+$ mono- or bilayers of urothelium are observed in *Col17a1*-KO (white arrows). The nucleus was stained using Hoechst (blue). White dotted lines represent the apical side of the urothelium. Immunofluorescence. Bars = 100 μm.

(F) Localization of ZO-1 (green) with OCLN (red) in RP 1 d after UUO. $ZO\text{-}1^+$ and $OCLN^+$ staining is observed at the apical portion of RP urothelium in *Col17a1*-KO, while the outcome is negative in WT (white arrows). In *Col17a1*-KO, $ZO\text{-}1^+$ staining shows an irregular pattern of upregulation (yellow arrowheads), and $OCLN^+$ results are also found in basal urothelial cells (white arrowheads). The nucleus was stained using Hoechst (blue). White dotted lines represent the apical side of the urothelium. Immunofluorescence. Bars = 100 μm.

(G) Localization of CD11b (green) with CXCL2 (red) in RP 1 d after UUO. $CD11b^+$ $CXCL2^+$ cells (arrowheads) are abundantly observed at the junction between the thin and thick RP urothelium in WT, whereas $CD11b^+$ cells are scattered under RP urothelium in *Col17a1*-KO and few co-express CXCL2. The nucleus was stained using Hoechst (blue). White dotted lines represent the apical side of the urothelium. Immunofluorescence. Bars = 50 μm.

(H) The number of $CD11b^+$ cells under thick RP urothelium 1 d after UUO. Each bar represents mean ± SE (n = 5–6). * indicates a significant difference compared with Cont (*$P < 0.05$). The Mann–Whitney *U*-test was used.

Fig. 8 Schematic illustration of the hypothetic mechanism through which obstructive uropathy induces urothelium disruption and COL17A1 expression

Normal RP and ureter comprise urothelial cells, fibroblasts, and smooth muscle cells. RPs are divided into thick RP connecting the ureter to the smooth muscle layer and thin RP connecting to the kidneys without a smooth muscle layer. There are some $CK14^+$ urothelial cells, particularly in the thin RP. After UUO, urothelial cell deciduation is observed (the early stage of UUO; 1 d and 4 d, in RP and ureter, respectively). In RP, urothelial cell deciduation and subsequent urine leakage occur with partial defects in the tight junction protein at the junction between thick and thin RP urothelium. Basal urothelial cells from the junction to the thick RP predominantly express COL17A1, and $CD11b^+$ cells migrate to connective tissue overlaid by $COL17A1^+$ proliferating urothelial cells beneath the urine-urothelial barrier disruption, which also express CXCL2. At this stage, $CK14^+$ urothelial cells are diminished. Fibrosis develops instead of cell deciduation and $CD11b^+$ cell migration at the late stage (4 and 7 d onwards in RP and ureter, respectively). There are abundant $COL17A1^+$ urothelial cells, which partially express CK14. The schematic illustrations represent RP urothelium.

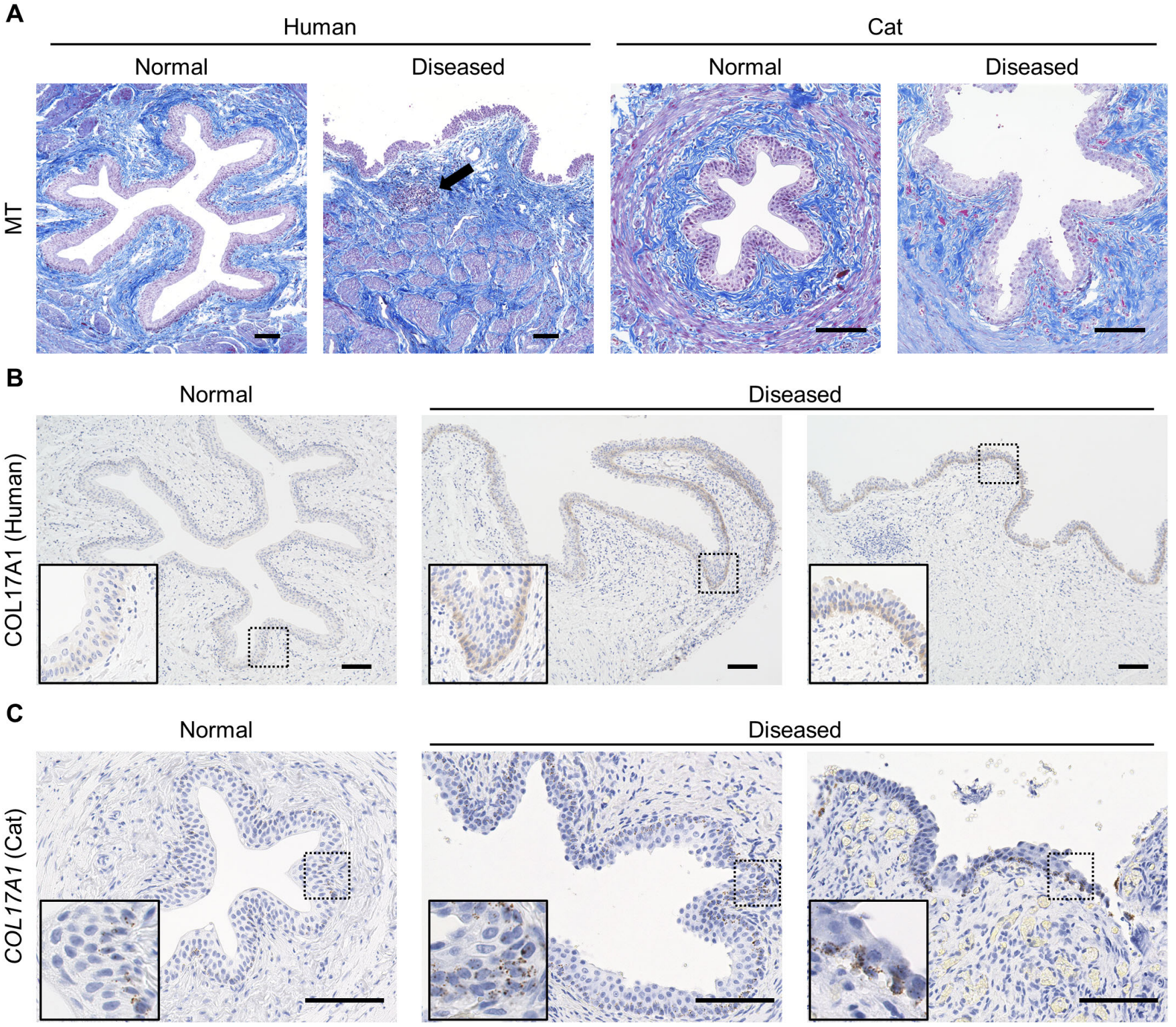
A
Human
Cat
Normal
Diseased
Normal
Diseased
MT
B
Normal
Diseased
COL17A1 (Human)
C
Normal
Diseased
COL17A1 (Cat)

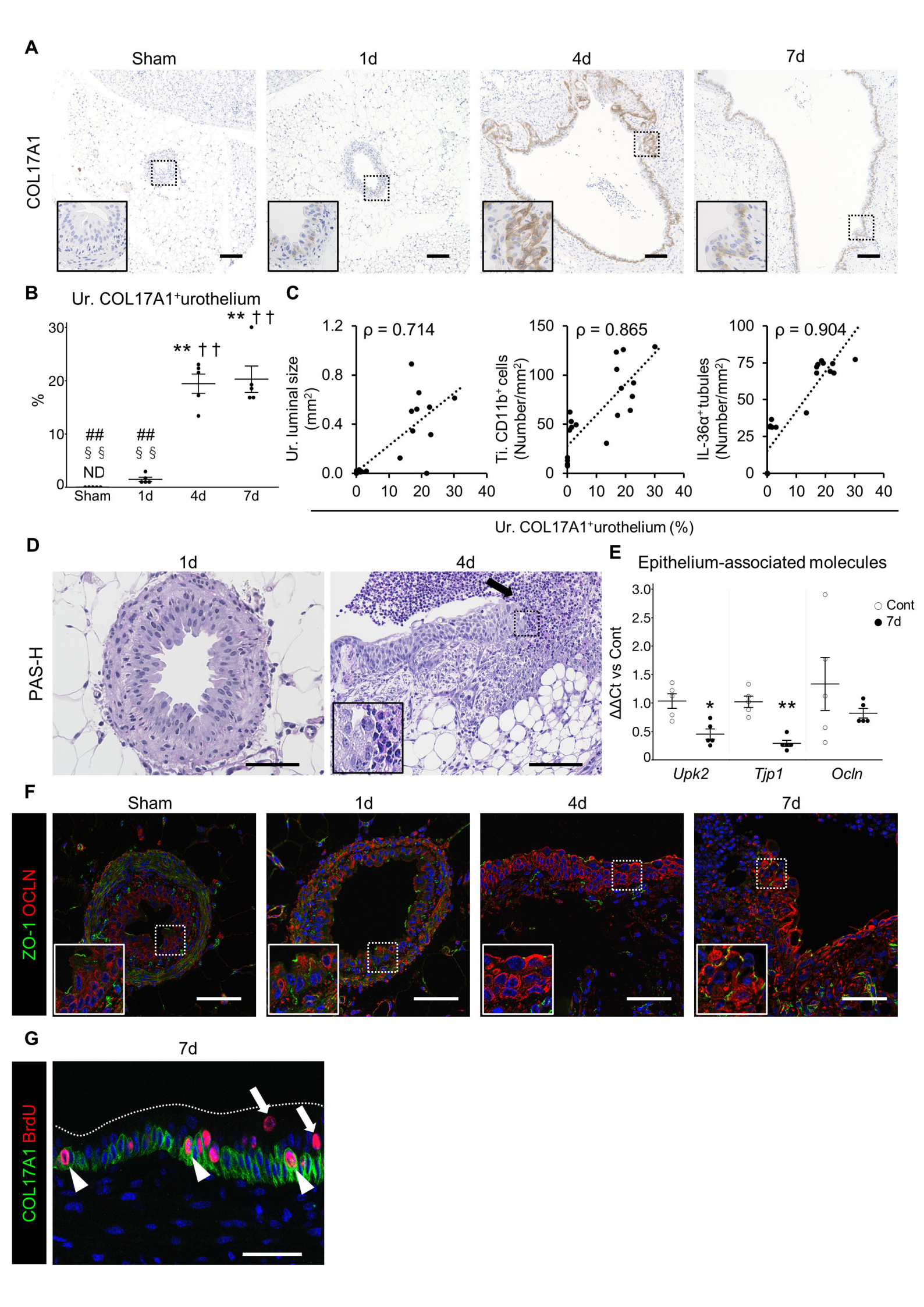
A
Sham
1d
4d
7d
COL17A1
B
Ur. COL17A1⁺urothelium
%
30
20
10
0
** † †
** † †
§§
§§
ND
Sham
1d
4d
7d
C
ρ = 0.714
ρ = 0.865
ρ = 0.904
Ur. luminal size (mm²)
Ti. CD11b⁺cells (Number/mm²)
IL-36α⁺tubules (Number/mm²)
Ur. COL17A1⁺urothelium (%)
D
1d
4d
PAS-H
E
Epithelium-associated molecules
ΔΔCt vs Cont
Cont
7d
Upk2
Tjp1
Ocln
F
Sham
1d
4d
7d
ZO-1 OCLN
G
7d
COL17A1 BrdU

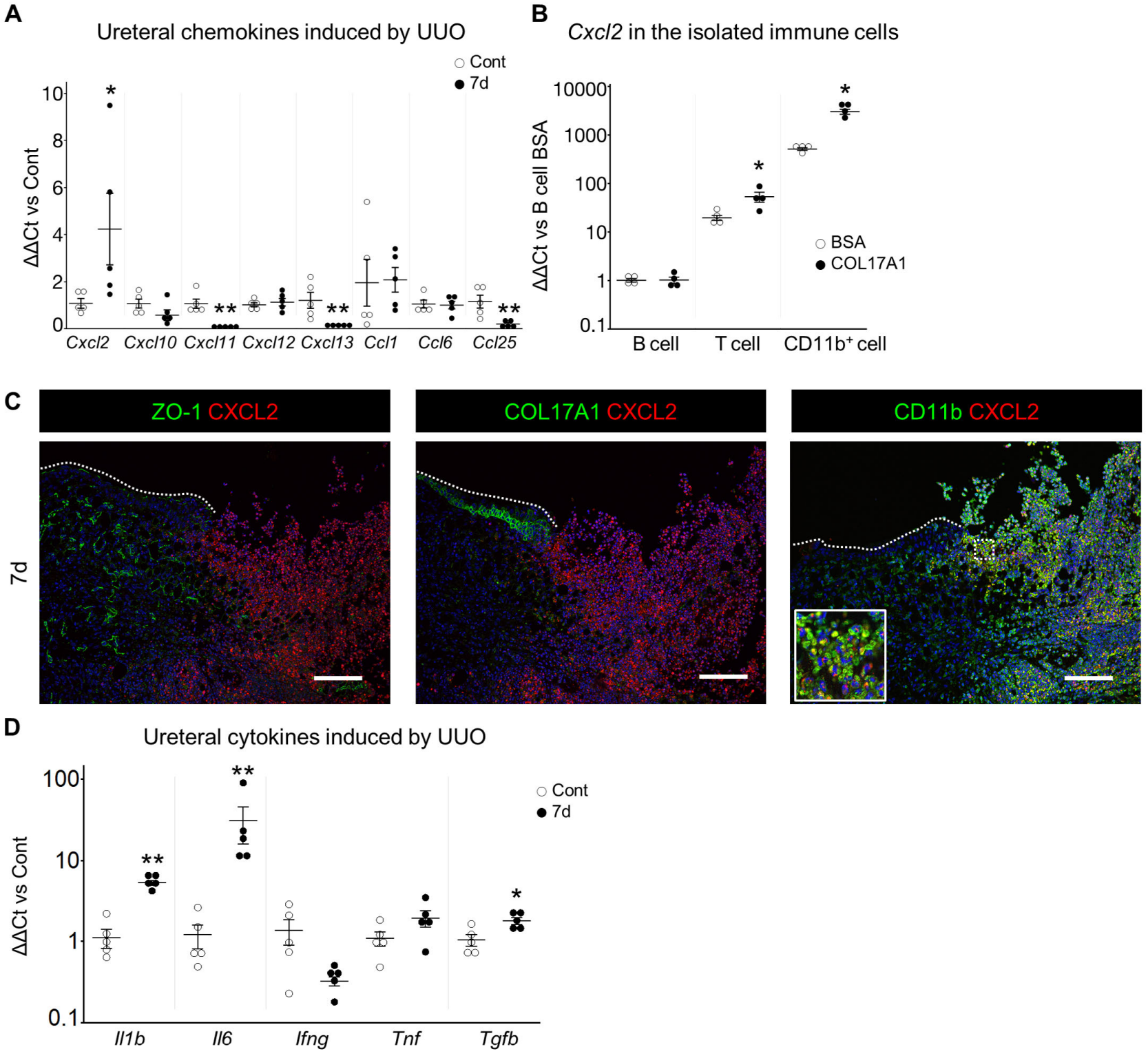
A
Ureteral chemokines induced by UUO
Cont
7d
ΔΔCt vs Cont
Cxcl2
Cxcl10
Cxcl11
Cxcl12
Cxcl13
Ccl1
Ccl6
Ccl25
B
Cxcl2 in the isolated immune cells
ΔΔCt vs B cell BSA
BSA
COL17A1
B cell
T cell
CD11b+ cell
C
ZO-1 CXCL2
COL17A1 CXCL2
CD11b CXCL2
7d
D
Ureteral cytokines induced by UUO
Cont
7d
ΔΔCt vs Cont
Il1b
Il6
Ifng
Tnf
Tgfb

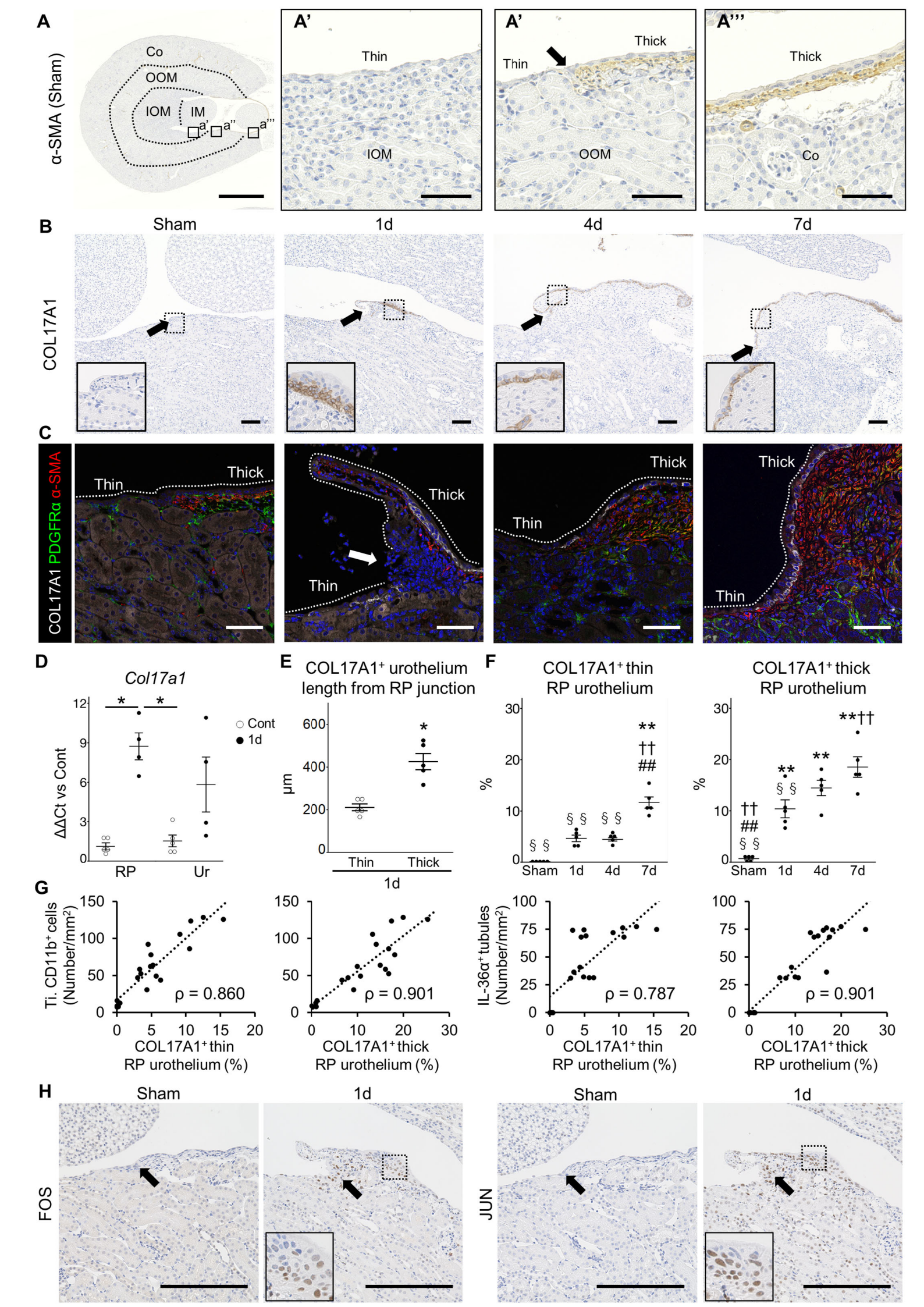
A
α-SMA (Sham)
Co
OOM
IOM
IM
a'
a''
a'''
A'
Thin
IOM
A'
Thick
Thin
OOM
A'''
Thick
Co
B
Sham
1d
4d
7d
COL17A1
C
COL17A1 PDGFRα α-SMA
Thin
Thick
Thick
Thin
Thick
Thin
Thick
Thin
D
Col17a1
ΔΔCt vs Cont
Cont
1d
RP
Ur
E
COL17A1⁺ urothelium length from RP junction
μm
Thin
Thick
1d
F
COL17A1⁺ thin RP urothelium
%
Sham
1d
4d
7d
COL17A1⁺ thick RP urothelium
%
Sham
1d
4d
7d
G
Ti. CD11b⁺ cells (Number/mm²)
ρ = 0.860
COL17A1⁺ thin RP urothelium (%)
ρ = 0.901
COL17A1⁺ thick RP urothelium (%)
IL-36α⁺ tubules (Number/mm²)
ρ = 0.787
COL17A1⁺ thin RP urothelium (%)
ρ = 0.901
COL17A1⁺ thick RP urothelium (%)
H
Sham
1d
FOS
Sham
1d
JUN

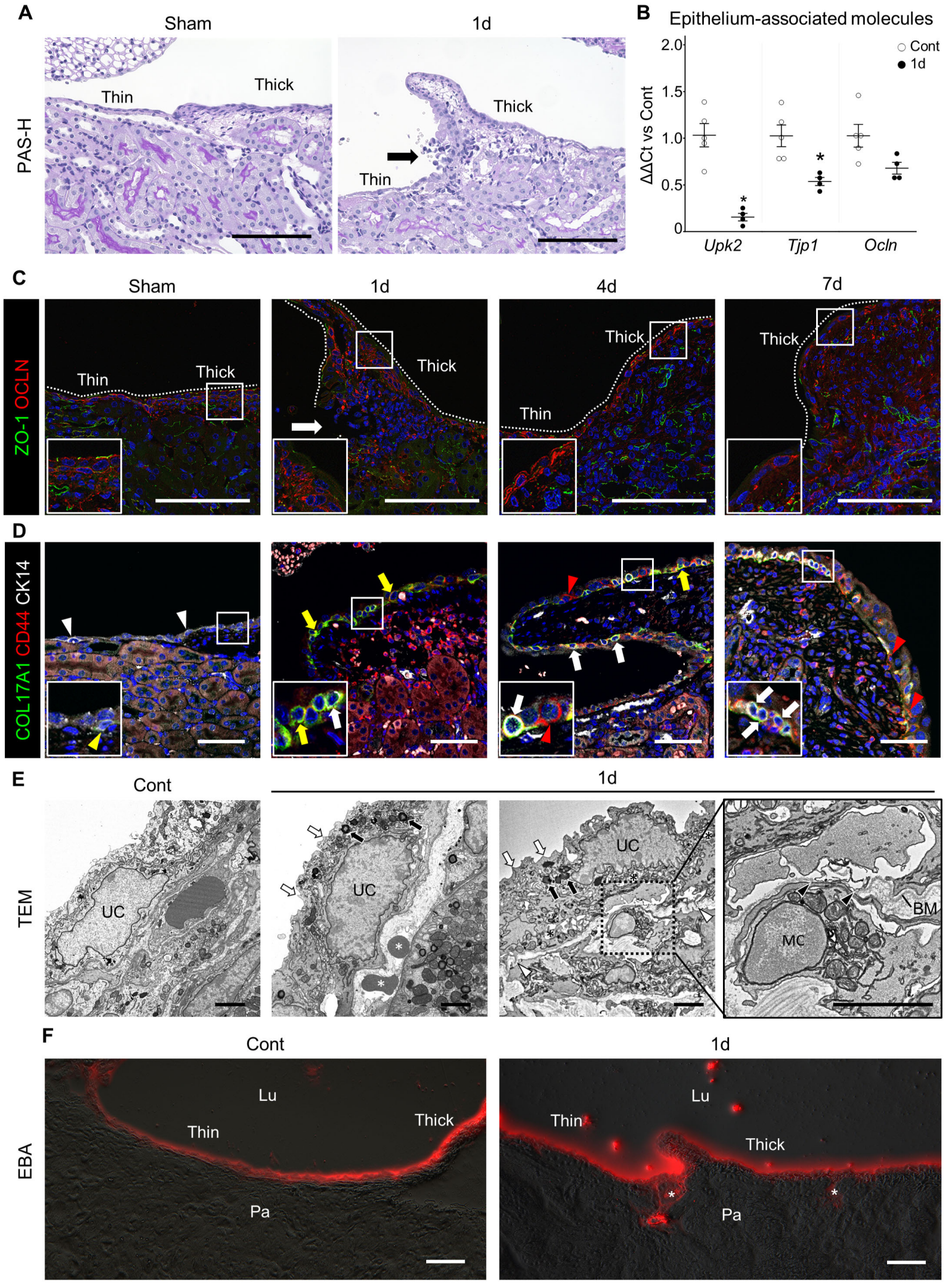
A
Sham
1d
PAS-H
Thin
Thick
Thick
Thin
B
Epithelium-associated molecules
Cont
1d
ΔΔCt vs Cont
2.0
1.5
1.0
0.5
0
Upk2
Tjp1
Ocln
C
Sham
1d
4d
7d
ZO-1 OCLN
Thin
Thick
Thick
Thick
Thin
Thick
D
COL17A1 CD44 CK14
E
Cont
1d
TEM
UC
UC
UC
BM
MC
F
Cont
1d
EBA
Lu
Thin
Thick
Pa
Lu
Thin
Thick
Pa

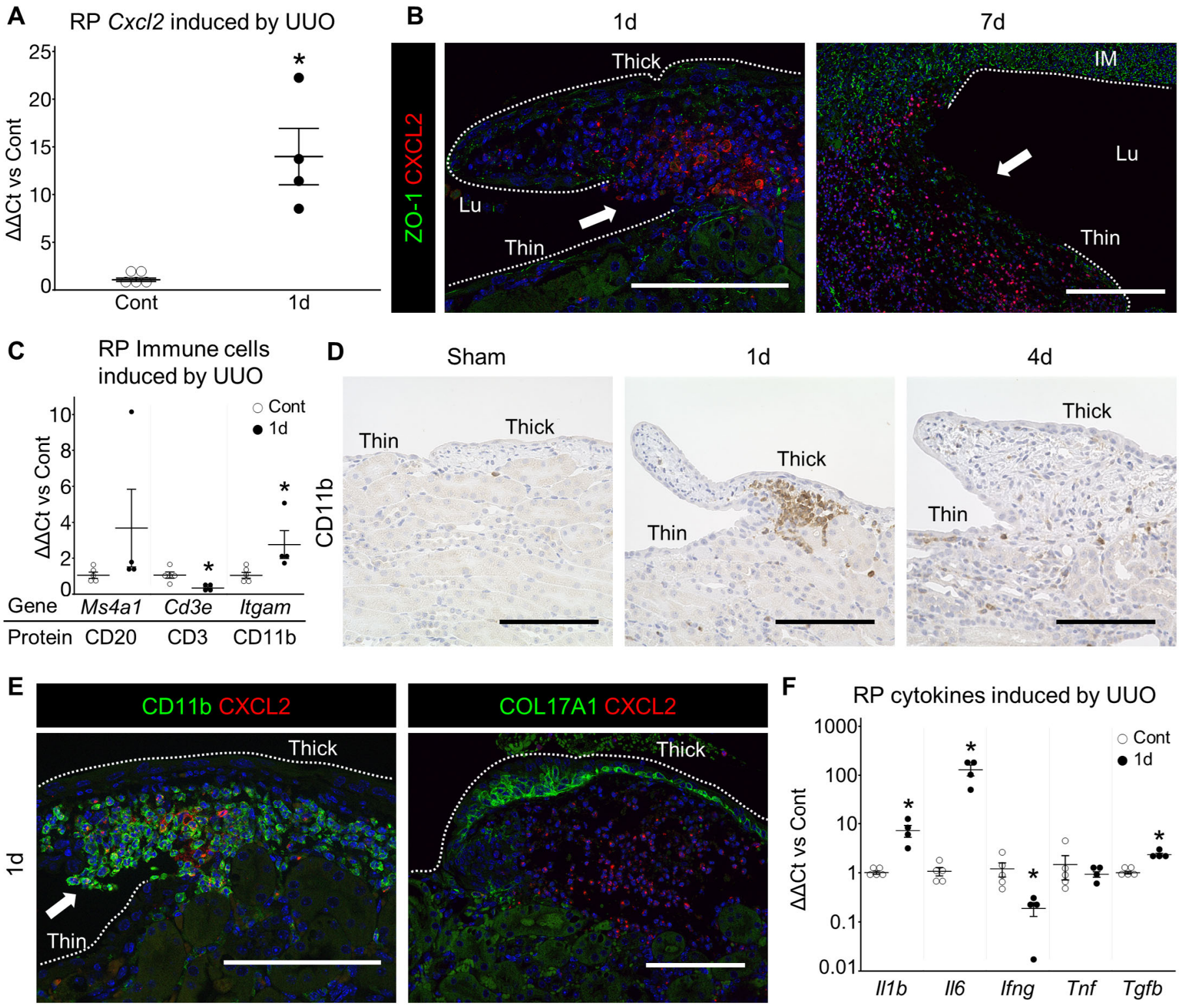
A
RP Cxcl2 induced by UUO
ΔΔCt vs Cont
25
20
15
10
5
0
Cont
1d
B
1d
7d
ZO-1 CXCL2
Thick
Lu
Thin
IM
Lu
Thin
C
RP Immune cells induced by UUO
ΔΔCt vs Cont
Cont
1d
Gene
Ms4a1
Cd3e
Itgam
Protein
CD20
CD3
CD11b
D
Sham
1d
4d
CD11b
Thin
Thick
Thick
Thin
Thick
Thin
E
CD11b CXCL2
COL17A1 CXCL2
1d
Thick
Thin
Thick
F
RP cytokines induced by UUO
ΔΔCt vs Cont
1000
100
10
1
0.1
0.01
Cont
1d
Il1b
Il6
Ifng
Tnf
Tgfb

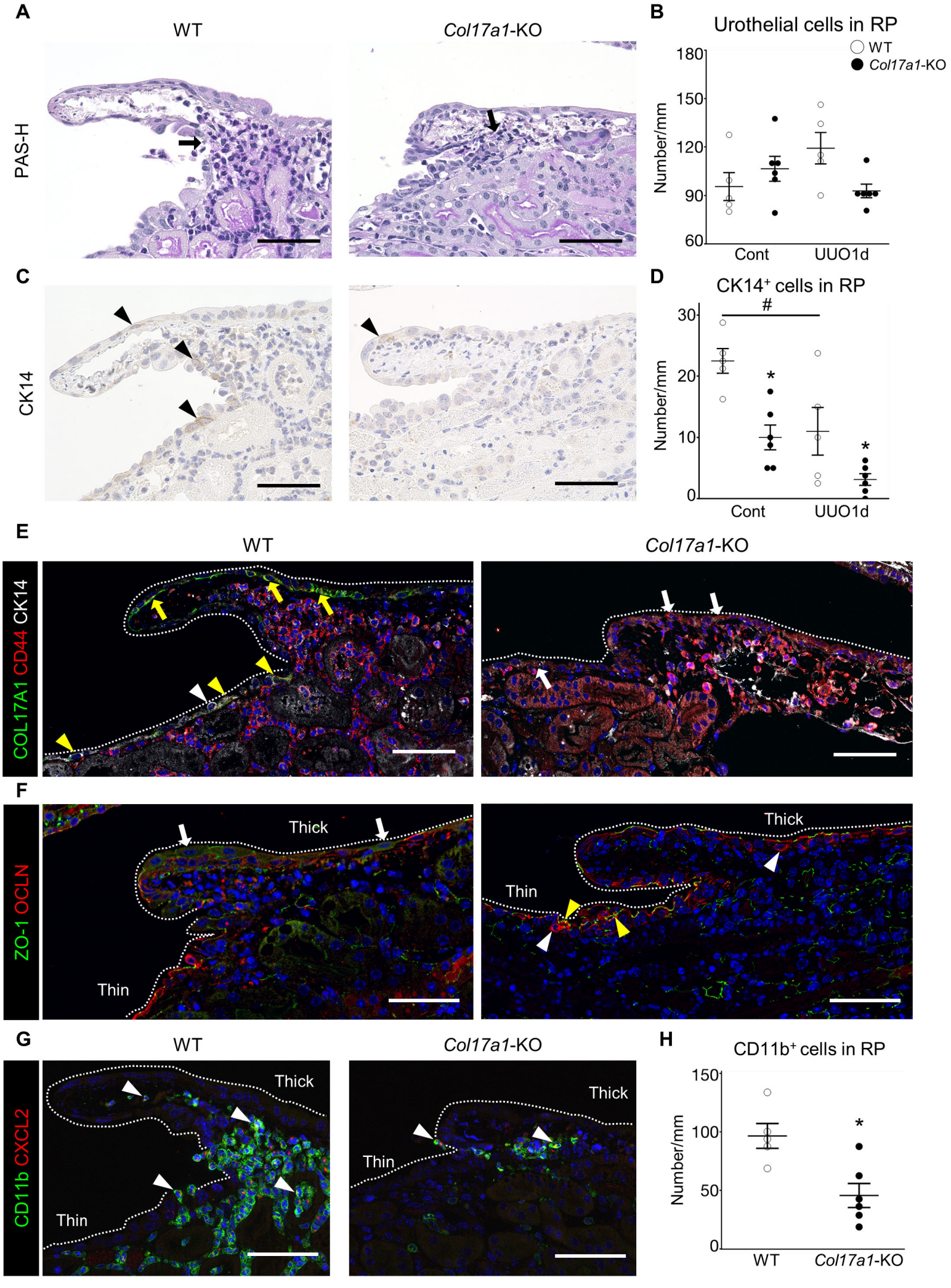
A
WT
Col17a1-KO
PAS-H
B
Urothelial cells in RP
WT
Col17a1-KO
Number/mm
180
150
120
90
60
Cont
UUO1d
C
CK14
D
CK14+ cells in RP
#
*
*
Number/mm
30
20
10
0
Cont
UUO1d
E
WT
Col17a1-KO
COL17A1 CD44 CK14
F
ZO-1 OCLN
Thick
Thin
Thick
Thin
G
WT
Col17a1-KO
CD11b CXCL2
Thick
Thin
Thick
Thin
H
CD11b+ cells in RP
Number/mm
150
100
50
0
*
WT
Col17a1-KO

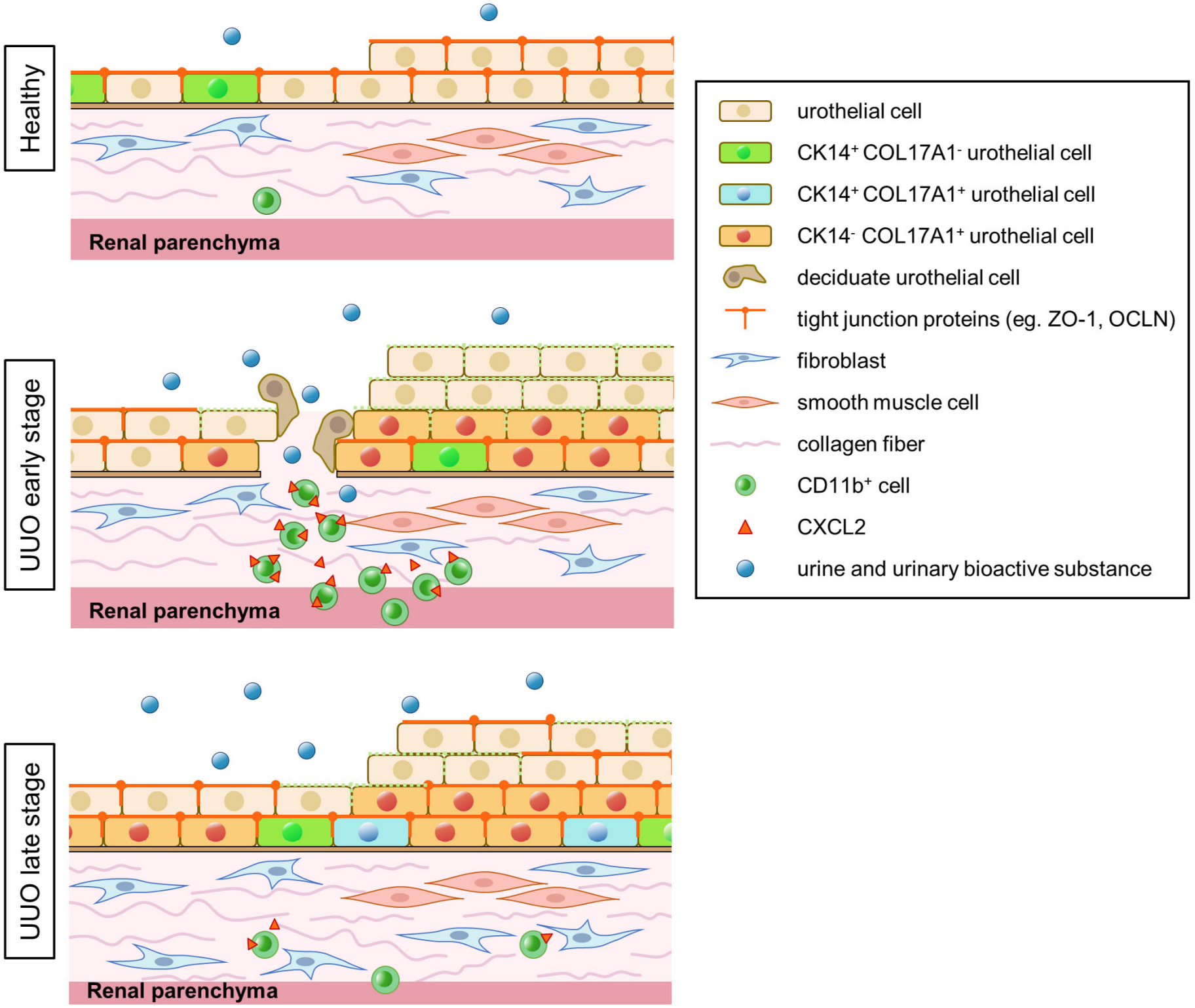
Healthy
Renal parenchyma
UUO early stage
Renal parenchyma
UUO late stage
Renal parenchyma
urothelial cell
CK14+ COL17A1- urothelial cell
CK14+ COL17A1+ urothelial cell
CK14- COL17A1+ urothelial cell
deciduate urothelial cell
tight junction proteins (eg. ZO-1, OCLN)
fibroblast
smooth muscle cell
collagen fiber
CD11b+ cell
CXCL2
urine and urinary bioactive substance